Drifting To Daylight

How Migration Routes for the Arctic Tern Are Influenced by Climate Change Induced Global Wind Pattern Changes

Frank Schippers 6215548 f.j.schippers@students.uu.nl

Supervisors KNMI: Nomikos Skyllas & Richard Bintanja

UU Examiners: Erik van Sebille & Michiel Baatsen

Contents

Abstract

Some Arctic tern populations migrate from Antarctic regions to Svalbard during boreal spring (March-May). During this migration, they encounter and are greatly influenced by the wind patterns over the Atlantic Ocean. Making use of tailwinds in the Atlantic Ocean, the migration route of Arctic terns has an S-shape. This study explored how climate change induced wind pattern changes in the Atlantic Ocean influence the migration route of the Svalbard population of Arctic terns. This was achieved by exploiting a least cost path (LCP) model using near surface wind (ERA5) and chlorophyll A (ESACCI-OC) data. First, a set of sensitivity experiments testing the impact of departure day and starting location were done. Then the model was fine-tuned and validated for an ensemble of four CMIP6 Earth System Models (ESMs) against the Arctic tern geolocator tracking data. In the present study, a total of 61 geolocators were used to log the migration paths of Arctic terns. Afterwards, future wind and chlorophyll A data from the ESM ensemble under four different climate scenarios (SSP119, SSP126, SSP245, and SSP585) were used to explore the changes in wind patterns and migration routes. The departure day was found to have a significant impact on the migration route. However, no clear departure window was observed. Furthermore, no significant changes in the migration route were found for all climate scenarios, though minimal changes were observed. Accordingly, no link between the expansion of the Hadley cell and changes in the migration route was found. Upgrading the model to 3D and increasing the spatial resolution could give more insight into migration routes and allow for a better representation of the complex wind pattern changes.

Keywords

Arctic Tern, Atlantic Ocean, Geolocator tracking, Least Cost Path Model, Wind Circulation, CMIP6

List of Abbreviations

ESM	Earth System Model
LCP	Least Cost Path
ERA5	European Centre for Medium-Range Weather Forecasts Reanalysis v5
ESACCI-OC	European Space Agency Climate Change Initiative Ocean Colour
CMIP6	Coupled Model Intercomparison Project 6
CanESM5	Canadian Earth System Model version 5
GFDL	Geophysical Fluid Dynamics Laboratory Earth System Model version 4
MPI	Max Planck Institute Earth System Model Low Resolution
KIOST	Korea Institute of Ocean Science & Technology
IPCC	Intergovernmental Panel on Climate Change
RMSE	Root Mean Squared Error

1. Introduction

Wind patterns play a crucial role in shaping the Earth's climate systems. The wind patterns, driven by the uneven incoming solar radiation and heating of the surface layer, distribute heat and moisture across the globe, influence weather patterns, and determine the global and regional climate (Hsu et al. 1997, Ferrari and Ferreira 2011, Laliberté et al. 2015). Climate change can cause these global and regional wind patterns to change in strength, spatial distribution, and frequency (Laliberté et al. 2015, Hu et al. 2018, Studholme and Gulev 2018, Staten et al. 2020, Gray et al. 2021, Deng et al. 2022). The recent IPCC AR6 report highlighted that climate change already affects our daily experiences in many ways and that changes are accelerating (IPCC AR6 2021). The increase in global temperature and precipitation is one of the major areas of interest within the field of climate change and is therefore relatively well understood. On the contrary, global wind pattern changes due to climate change receive far less attention, even though it could have a significant impact on weather patterns, agriculture, and ecological systems (Chakraborty et al. 2015). Furthermore, Earth System Models (ESMs) show a lack of consensus in global wind pattern changes (Grise and Davis 2020, Smith et al. 2020). This has been observed by the IPCC AR5 report, stating that: "*confidence is low in changes in surface wind speed over the land and over the oceans owing to remaining uncertainties in data sets and measures used.*" (IPCC AR5 2014). Accordingly, future wind pattern changes is an area of interest in the field of climate science.

The last decades of the 20th century have seen a terrestrial stilling of near surface winds in the northern mid-latitudes of about -0.3 m/s in 2005 compared to 1975 (Bichet et al. 2012, Zeng et al. 2019). After the turning point in 2010 however, near surface wind speeds were intensifying again, with an increase of about 0.17 m/s between 2010 and 2017 (Zeng et al. 2019). Notably, both the increasing near surface windspeeds after 2010, and the terrestrial stilling in the decades before can likely be attributed to decadal variability in large-scale ocean-atmosphere oscillations (Zeng et al. 2019). The ways in which global and regional wind patterns may change in the future depends on multiple factors such as global atmospheric circulation, turbulent friction, and surface friction (Zhang et al. 2019). Regionally, the abundance of land masses and oceans, topography, and the latitude on the globe can greatly impact the pattern (Huang et al. 2019). To understand and project how near surface winds will change in the future, not only the ocean-atmosphere oscillations are important (Smith et al. 2020). Some of the above-mentioned factors, such as global atmospheric circulation, turbulent friction, and latitudinal influence, are changing due to climate change and can hence also influence the near surface wind patterns of the future. The importance of latitude is especially interesting, as the current global wind patterns related to specific latitude bands might shift poleward in the future (Studholme and Gulev 2018, Grise and Davids 2020).

A changing wind pattern will affect the climate and weather and therefore affects both human life and other species. This is especially relevant for avian species migrating through the atmosphere, ranging from small insects to raptors (Kemp et al. 2012, McLaren et al. 2012, Hensz 2015, Chapman et al. 2016, Shamoun-Baranes et al. 2017, Hromádková et al. 2020). The extent to which a species will be impacted by changes in wind patterns depends on where the species occurs and on their migration route. One of the species that might be impacted most is the Arctic tern, also known as the Sterna paradisaea (see Figure 1) (Hensz 2015, Hedenström and Akesson 2016, Hromádková et al., 2020). The Arctic tern is a migratory bird species that lives at the high latitudes. Surviving at the high latitudes with tough weather conditions and low temperatures is difficult. The conditions to survive and procreate are optimal in the summer as temperatures are higher, days are longer, and food is more abundant. However, summer at these latitudes only last a few months. Therefore, the Arctic terns migrate twice a year between the two polar regions. Between March and May they migrate

from the Antarctic to regions north of the Arctic Circle such as Greenland or Svalbard (Hensz 2015, Hromádková et al. 2020). When autumn arrives in these regions they migrate back to the Antarctic, just in time for austral summer (Hensz 2015, Hromádková et al. 2020). While doing so, Arctic terns experience sunlight about 80% of the time, significantly more than any other species (Hromádková et al. 2020).

Figure 1. An Arctic tern (Sterna paradisaea). Photo credit: Akhil Pradesh & Nomikos Skyllas

While experiencing both summers at the different hemispheres with higher temperatures and more daylight compared to winter gives big advantages, the two migrations can span up to a total of 80.000 kilometers and are a serious effort for the Arctic terns (Egevang et al. 2010). To complete one migration, they fly over the entire span of the Atlantic Ocean and experience the winds from the polar, Ferrel and the Hadley cells. To successfully migrate in time for the breeding season, wind conditions are of vital importance as they increase the migration speed and decrease the required amount of energy needed for the migration (Egevang et al. 2010, Hensz 2015, Hedenström and Akesson 2016, Hromádková et al. 2020). Besides the importance of favorable winds, food availability is also a key factor during the Arctic tern migration, as Arctic terns are drawn to upwelling areas with high food availability during their migration to refuel (McKnight et al. 2013, Hensz 2015, Hedenström and Akesson, 2016, Hromádková et al. 2020). Arctic terns mainly predate on squids, shellfish and various small fish species (Ashmole et al. 1968). Since Arctic terns forage mid-flight and mid-migration, they often migrate at an altitude of less than 100 meters above the surface (Ashmole et al. 1968, Alerstam et al. 2007). However, when not foraging, Arctic terns can fly at higher altitudes of up to five kilometers and make use of stronger tailwinds (Alerstam and Gudmundsson 1999, Alerstam et al. 2007).

All in all, Arctic terns are dependent on favorable wind patterns for their annual migrations (Egevang et al. 2010). Especially the Svalbard population of Arctic terns is very much impacted in their migration by the wind patterns over the entire Atlantic Ocean and can therefore serve as a proxy for those wind patterns (Egevang et al. 2010, Morten et al. 2023, Skyllas et al. 2023). Thereupon, while looking at the changes in the Atlantic wind pattern, induced by climate change, one might expect to also see changes in the migration route of this population of Arctic terns. This paper sets out to answer how climate change induced wind pattern changes in the Atlantic Ocean influence the migration routes of the Arctic tern boreal spring migration (March-May) to Svalbard. This issue will be explored by exploiting a least cost path (LCP) model that is validated against Arctic tern tracking data

in the present day, based on the model introduced by Skyllas et al. (in preparation). However, whereas Skyllas et al. (in preparation) focused on the seasonal mean and the emerging mean flyway of the population, this study will shift to a daily resolution and explore the randomness of the population by looking at individual birds. First we compare the resulting interindividual variability to the interindividual variability from the tracking data. Secondly, future wind data from four different Earth System Models (ESMs) under four different climate scenarios (Shared Socioeconomic Pathways; SSP119, SSP126, SSP245, SSP585) will be used to explore the changes in wind patterns and migration routes. In the next sections, first a theoretical background for the research will be given. Then the data used for the LCP model in both present and future will be described, after which the LCP model will be explained in more detail. Afterwards the results from the experiments with the LCP model will be shown. Finally, the results and their implications for the research area will be discussed.

2. Theoretical Framework

2.1. Atmospheric Circulation

To understand how the wind pattern might change in the future, one has to understand the global wind pattern and its mechanisms in the present day. The earth is rotating eastward around its axis. This rotating motion results in a force for everything that is in motion in the meridional direction, also known as the Coriolis force. As a result of the Coriolis force and the conservation of angular momentum, air parcels moving to higher latitudes will drift to the east (Herrera and Morett 2016). Alternatively, an air parcel moving to lower latitudes will drift westward. Whether an air parcel moves towards or away from the equator mainly depends on the latitude of the air parcel. The global atmospheric circulation is driven by temperature differences caused by differences in solar insolation (Hoskins et al. 2020, Hoskins and Yang 2021). At the equator there are relatively high temperatures, whereas the poles exhibit low temperatures resulting in a meridional temperature gradient. This temperature gradient is the main driver of the atmospheric circulation. The general atmospheric circulation can be divided into three interacting components: a zonally symmetric circumpolar vortex (see also: Waugh et al. 2017), a zonally symmetric meridional circulation (see also: Randall 2015), and zonal asymmetries caused by eddies and planetary waves (see also: Wills et al. 2019). The second component, the zonally symmetric meridional circulation, consists in both hemispheres of three different circulation cells, each with its own latitude band: the Hadley cell, the Ferrel cell, and the polar cell (see Figure 2).

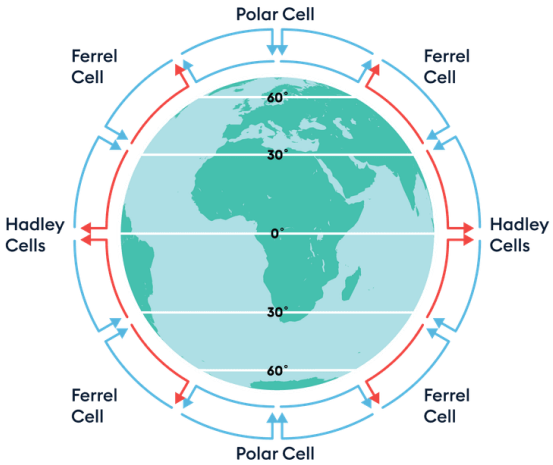

Figure 2. Overview of the basic zonally symmetric meridional atmospheric circulation pattern with the Hadley cell, the Ferrel cell, and the polar cell (from Encounter Edu).

The first is the thermally direct Hadley cell, which reaches approximately from the equator until 30° north or south. The Hadley cell is a convective circulation caused by uneven solar heating of earth's surface. Near the equator the surface is heated the most and the warm air rises due to buoyancy, creating a low-pressure zone at the surface. While rising, the air cools off by releasing latent heat, getting denser and cooler. At the upper levels of the troposphere near the equator, the relatively cold and dry air results in a pressure gradient with upper troposphere levels at higher latitudes (Randall 2015, Hoskins et al. 2020, Hoskins and Yang 2021). This pressure gradient leads to a poleward flow at the upper layer of the troposphere. At the edge of the Hadley cell, at around 30°, the subtropical Jetstream forms as a result of angular momentum conservation and the influence of eddies (Archer et al. 2008, Hoskins et al. 2020, Hoskins and Yang 2021). Around 30° the cool and dry and thus dense air descends towards the surface creating a high-pressure zone at the surface. This high-pressure area, together with the low-pressure area at the surface near the equator, form a pressure gradient leading to an equatorward flow at the surface and a westward shift due to the Coriolis effect. These winds are known as the trade winds.

Secondly, there is the polar cell which spans from 60° until the poles. The polar cell, just like the Hadley cell, is thermally direct. Relatively warm and moist air masses undergo convection and ascend at around 60° to the Tropopause and move towards the pole (Randall 2015). The air masses cool off while moving poleward, thereby increasing their density. At the poles, the air descends to the surface creating a high-pressure area. The surface pressure gradient results in an equatorward flow, which shifts westward due the Coriolis effect. These surface winds complete the circulation of the polar cell and are known as the polar easterlies.

In between the Hadley and polar cells, the Ferrel cell extends from 30° to 60°. The Ferrel cell is thermally indirect and is mainly driven by the energy of the Hadley cell and the Polar cell (Randall 2015). The descending air from the Hadley cell at 30° creates a high-pressure area. The pressure gradient between 30° and higher latitudes results in a poleward surface flow, which then shifts eastward due to the Coriolis effect. These surface winds are known as the westerlies. At about 60°, the relatively warm and moist air meets the relatively cold and dry air from the polar easterlies at the polar front. The temperature differences at the polar front are the main reason for the polar Jetstream that is present here (Archer et al. 2008). The warm and moist air ascends creating a low-pressure zone at the surface. At higher levels of the troposphere, the air mass cools off and flows equatorward due to a pressure gradient. The Ferrel cell is a lot weaker than the Hadley cell, which leads the prevailing westerlies to not be as consistently present as the trade winds. This system consisting of three circulation cells are the basics for the prevailing zonally symmetric surface wind directions.

Regionally, however, other factors such as mountains and other topography, the abundance of land masses and oceans, turbulence, and ocean-atmosphere oscillations can change this pattern (e.g. Walker circulation, El Niño-Southern Oscillation). Especially in the mid-latitudes, zonally asymmetric turbulences in the atmosphere play a key factor in the circulation (Grotjahn 2002, O'Brien 2019). As mentioned in the section about meridional circulation, the zonally symmetric meridional circulation mainly comes from the rotation of the earth and the conservation of angular momentum. However, the rotation of the earth is not the only factor for angular momentum and vorticity, the swirling motion of geophysical fluids. The absolute vorticity consists, besides the planetary vorticity from the rotation of the earth, of the relative vorticity (wind shear and curvature) (Grotjahn 2002, O'Brien 2019). Finally, the potential vorticity depends on the absolute vorticity and the stratification. Potential vorticity, just like angular momentum, is a conserved quantity (Grotjahn 2002, O'Brien 2019). The baroclinic instabilities in the mid-latitudes come from this conservation of the potential vorticity.

Baroclinic instabilities and Rossby waves arise when potential vorticity anomalies interact and mix, while potential vorticity is conserved (Grotjahn 2002, O'Brien 2019, Wills et al. 2019, Hoskins and Yang 2021). In the baroclinic instability zone in the mid-latitudes, Rossby waves and eddies form, giving rise to high variability in pressure, temperature, and wind patterns (Grotjahn 2002, O'Brien 2019, Wills et al. 2019). The abundance of eddies is the reason why the westerlies are also called prevailing westerlies, as wind patterns are more variable in the mid-latitudes compared to the Hadley and polar cell (Grotjahn 2002, Randall 2015). The eddies are also important for the circulation of heat and air mass, as the mass flux from the eddies is larger than the mass flux of the Ferrel cell (Grotjahn 2002). How this system of global atmospheric circulation will change in the future depends on the ocean-atmosphere oscillations and shifts due to climate change (Grise et al. 2019, Zeng et al. 2019, Staten et al. 2020).

2.2. Changes in Atmospheric Circulation

According to previous research from Staten et al. (2018), Studholme and Gulev (2018), and Grise and Davis (2020) the Hadley cell has expanded over the past 40 years and has shifted poleward 0.1° - 0.5° of latitude per decade. This expansion of the Hadley cell is driven by different rates of warming due to climate change across the earth (Hu et al. 2018). Satellite observations indicate a stronger warming in the subtropics than in the tropics (Hu et al. 2018). This leads to a poleward shift of the baroclinic instability zone (Lu et al. 2007, Hu et al. 2018). Lu et al. (2007) suggest that this poleward shift of the baroclinic instability zone is caused by in an increase subtropical static stability. However, Hu and Zhou (2010) argue that a decrease of vertical wind shear in the subtropical region is more important for the poleward shift of the baroclinic instability zone. This expansion of the Hadley cell is likely to be stronger during summer and autumn in the respective hemisphere (Grise et al. 2018, Hu et al. 2018, Staten et al. 2018). It is still uncertain whether and how the strength of the Hadley cell will change as there is no consensus between ESMs and Global Circulation Models (Hu et al. 2018). D'Agostino and Lionello (2016) and Huang et al. (2019) found that the trade winds in the Hadley cells may be intensifying, whereas Hu et al. (2018) point out that some reanalysis datasets show strengthening of the Hadley circulation, albeit maybe artificial. In their study, ERA-40 had the largest increase in Hadley circulation strength, but this trend was found to be artificial as it was caused by an unrealistic increase in tropical precipitation (Hu et al. 2018). Notably, Hu et al. (2018) also highlight that simulations with GCMs show a weakening of the Hadley circulation under climate change. In addition to changes in the Hadley circulation, the Ferrel cell might also shift poleward under global greenhouse warming (Abell et al. 2021). In their palaeoclimatological study, Abell et al. (2021), examined dust particles in deep sea sediments and used them as proxy for surface winds in the past. Their results show that in the Pliocene and Pleistocene, during which the global surface temperature was significantly higher than now, the westerlies from the Ferrel cell extended to higher latitudes and were weaker than they are in the present. Furthermore, Gray et al. (2021) found that the poleward shift and weakening of the westerlies during deglaciation closely matches the rises of atmospheric CO_2 concentration. This suggests that the Ferrel cell might shift poleward and decrease in strength with the rise of the global surface temperature.

2.3. Arctic Tern Migration Strategies

According to ecological theory, Arctic terns use the wind and food availability to find an 'optimal' migration path, in other words, the most time- or energy-efficient migration path (Alerstam 2011). Through trial-and-error and natural selection each population of Arctic terns has developed their own migration path (Alerstam 2011). A tailwind both saves a lot of energy and increases the speed compared to the ground (groundspeed) and is thus important in minimizing energy and time. Alerstam and Gudmundsson (1999) found a mean increase in groundspeed of 4.6 m/s when flying

with tailwinds, whereas the airspeeds were often lower. However, since the wind direction changes throughout the migration, there are multiple flying strategies the birds could use to make the most of the atmospheric conditions, see Figure 3 (Liechti 2006, Chapman et al. 2011). The first option is passive downstream transport (Chapman et al. 2011), where the Arctic tern does not fly itself but completely depends on the wind. The groundspeed and direction are exactly the same as the wind. Secondly, there is active downstream orientation (Chapman et al. 2011). In this strategy the bird flies in the exact same direction as the wind (full tailwind). The groundspeed is then a simple sum of the windspeed and the airspeed of the Arctic tern. The third strategy is compass-biased downstream orientation (Chapman et al. 2011). This strategy is similar to the active downstream orientation, except for the fact that the bird deviates its own flying direction a bit towards the direction of the destination. The flying direction is between the wind direction and the destination direction. The fourth strategy is full drift (Chapman et al. 2011). In this strategy, the flying direction of the tern is simply always faced towards the destination, irrespective of the wind. While the tern is headed towards the destination, the wind direction means the tern drifts off the right track. The fifth strategy is complete compensation (Chapman et al. 2011). In this strategy, the tern adjusts its heading in such a way that the track direction, consisting of both the fly direction and wind direction, is exactly pointed towards the destination. In other words, the tern compensates for the direction and speed of the wind so that it flies directly in a straight line towards the destination. The sixth strategy is a mix of drifting and compensating: partial drift, or partial compensation (Chapman et al. 2011). The tern partially compensates for the wind direction, but not completely. This causes the tern to still drift a bit with the wind direction. The seventh flying strategy is overcompensation (Chapman et al. 2011). In this case the Arctic tern compensates more than the flow drifts the Arctic tern away from the goal. The eighth and final strategy is upstream orientation (Chapman et al. 2011). The tern flies at the opposite direction of the wind and has full headwinds. This is mainly used over short distances to reach the target when other strategies are not possible to reach the target.

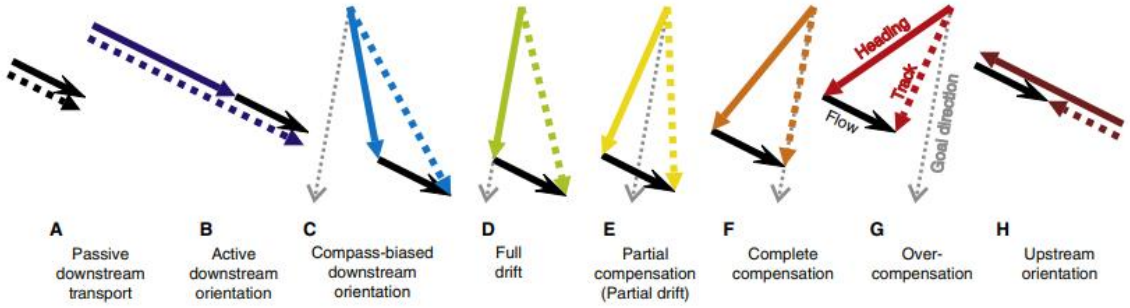

Figure 1. Different flying strategies, from Chapman et al. (2011). Each panel (A-H) has a schematic overview of one of the eight flying strategies described in Chapman et al. (2011). The solid black arrows depict the wind vectors. The solid colored arrows depict the heading and the air speed of the Arctic tern. This is all the work done by the Arctic tern itself. The dotted colored arrows depict the track and the ground speed of the Arctic tern. This is a sum of the wind vector and the heading vector: the total movement of the Arctic tern compared to the surface. The grey dotted arrows depict the direction of the final destination of the migration.

While migrating, there is not one single best strategy for the entire migration (Shamoun-Baranes et al. 2006, Chapman et al. 2011, Kemp et al. 2012, McLaren et al. 2012, Chapman et al. 2016, Hedenström and Akesson 2016, Shamoun-Baranes et al. 2017). Some sections require different strategies than other sections. While the downstream orientation costs the least amount of energy, the amount of time it takes to get to the destination can become a lot longer, if at all possible to reach the destination with solely downstream orientation. The best strategy during the migration is a subtle balance between minimizing both time and energy (Liechti 2006, Chapman et al. 2011, Kemp et al. 2012, McLaren et al. 201, Chapman et al. 2016, Hromádková et al. 2020). What is most

important in this balance depends on the population and migration route. During the boreal spring migration (March-May) populations that fly to Greenland and Svalbard prefer to minimize the energy while keeping the migration time as low as possible (Egevang et al. 2010, Hensz 2015, Hromádková et al. 2020). The population that nests in the North Sea area however, seems to put more emphasis in minimizing time and is therefore more likely to use full compensation (Fijn et al. 2013). Arriving too late would risk a phenological mismatch, and thereby causes the departure window and migration time to be strictly confined (Mcknight et al. 2013). In the boreal autumn migration (between the end of August and the start of November), both populations put less emphasis on minimizing the energy and time (Egevang et al. 2010, Fijn et al. 2013, Hensz 2015). They take more time to forage and eat at staging sites on the way back and therefore have more energy to spend and care less about the wind direction. Taking these migration strategies and the atmospheric conditions into account, populations have developed mean migration flyways that they more or less follow for many years. These migration flyways differ per population. To understand these flyways and the influence of the atmospheric conditions on them, studies have been carried out to monitor these flyways using tracking devices, climate data, and models.

3. Methodology

3.1. Tracking Data

Arctic tern tracking data was used to validate the model and its performance. A total of 61 geolocators logging the paths of Arctic terns were used in this study (see Figure 4). Geolocators were used in favor of GPS trackers, despite the superior accuracy, spatial resolution, and availability of an altitude meter on the latter, since up until this year GPS trackers were too heavy for Arctic terns to carry (Morten et al. 2023). The geolocators were attached to the Arctic terns between 2012 and 2016 at Svalbard (Skyllas et al. 2023). The geolocators estimated the locations twice per day by capturing the incoming light intensity. Using the length of the day and time of sunrise and sunset, a rough estimate of location with an uncertainty of ~185 km could be made (Phillips et al. 2004). Since the geolocators need a diurnal cycle to estimate the location, they can only estimate the position up until the point where there is 24 hours of sunlight per day. This was approximately around Iceland for the northern hemisphere. In addition, a 10-day period before and after the equinox was excluded, as the day length is similar around the globe for that period (Skyllas et al. 2023). Furthermore, resting and refueling at staging areas was excluded from the data according to Skyllas et al. (2023). For this study only the boreal spring migration (March-May) from the Arctic tern population that nests in the Svalbard area was taken into account, since this specific migration is most reliant on the wind pattern over the Atlantic Ocean. For a more detailed overview of the tracking data, see Skyllas et al. (2023).

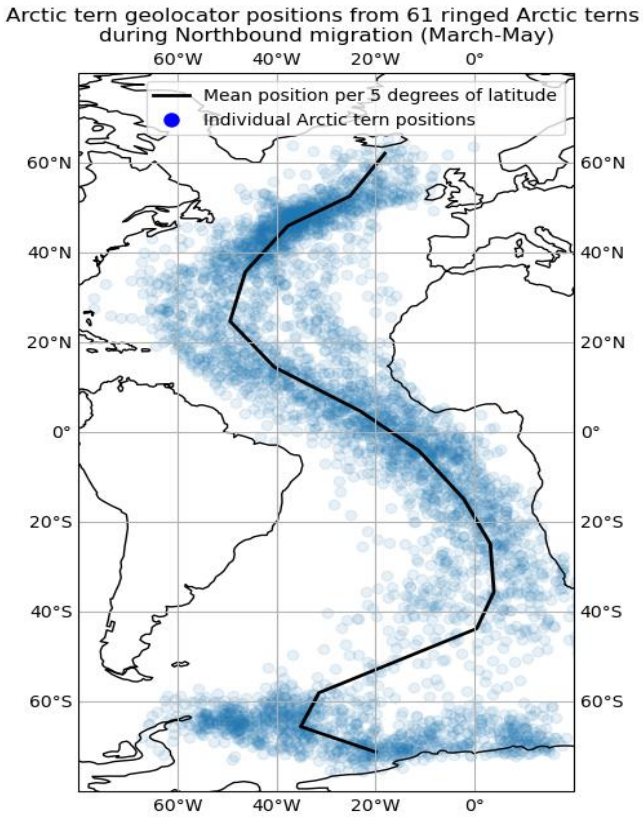

Figure 2. The Arctic tern tracking data used in the present study. In blue: positions of individual birds. In black: the mean position of the 61 ringed Arctic terns, taken per five degrees of latitude. All Arctic terns were captured, ringed, and recaptured in Svalbard between 2012-2016. The data was filtered by excluding all datapoints outside the northbound migration period (March-May). Furthermore, datapoints during the equinox or in areas with 24 hours of light per day were excluded.

3.2. Wind

The present study has used ECMWF Reanalysis v5 (ERA5, Hersbach et al. 2018) for the wind conditions of the past years. A single altitude level for the wind conditions had to be chosen, since the LCP model used in the present study only has two dimensions: zonal and meridional. Since the Arctic terns often forage in midflight during their migration, the surface level wind (10m) was chosen and the zonal (u10) and meridional (v10) components of the surface wind were used. The climate is usually described as mean weather conditions over a period of 30 years (IPCC 2022). Accordingly, a period of 30 years was chosen to reflect the climate conditions (now and also for the future time periods). However, since chlorophyll A data was only available from 1998 onwards (see 3.3. Chlorophyll A), this study has taken a period of 25 years: 1998-2022. The original ERA5 data had a spatial resolution of 0.25° and an hourly temporal resolution. Since the LCP model is validated against the Arctic tern tracking data with low spatial accuracy, ~185km (Phillips et al. 2004), and daily temporal resolution, the ERA5 wind data was regridded bilinearly into a 1° × 1° spatial resolution and a daily temporal resolution using Climate Data Operator (Schulzweida 2021). After that the area of interest, the Atlantic Ocean (80°W – 20°E and 80°S -80°N), was selected.

3.3. Chlorophyll A

As discussed previously in the introduction, Arctic terns from the Svalbard population need both favorable wind conditions and food during their migration. They often forage and fish during flight, which requires the abundance of fish, shellfish, or other sources of food. Since neither nekton nor plankton data was available for both historical and future scenarios, chlorophyll A was used.

Chlorophyll A is a good proxy for plankton concentration and can therefore show areas with high productivity and food availability (Bellido et al. 2008, Witman et al. 2008, Canion et al. 2013, Druon et al. 2019). ESA Climate Change Initiative Ocean Colour v6 (ESACCI-OC, Sathyendranath et al. 2023) chlorophyll A was used to estimate the chlorophyll concentration. The original spatial resolution of ~4km was downscaled to 1° × 1° to match the wind data. Since the temporal resolution of 8 days had significant gaps in the data due to a lack of satellite coverage, the present study chose to use a monthly resolution. The monthly resolution of chlorophyll A concentration was mainly used to indicate high productivity areas and chlorophyll A concentrations do not fluctuate as much as changes in wind since chlorophyll builds up over weeks and shows seasonal cycles (Winn et al. 1995, Lavigne et al. 2015).

3.4. ESMs

Modelling the Arctic tern migration routes in the future requires both wind data and chlorophyll A data. To better compare the current results to the future migration routes it would make sense to use the five ESMs that have wind patterns which are most comparable to that of ERA5 as described in Skyllas et al. (2023). However, none of those ESMs had chlorophyll A data available for future runs. Instead, the ESMs were selected from CMIP6 on data availability. Specifically, suitable ESMs should have both chlorophyll A, in at least monthly resolution, and the surface wind components, in at least daily resolution, available. Moreover, they should have historical runs to validate the ESMs to the present and historical years from ERA5 and ESACCI-OC. Finally, the ESMs should have at least two of the following climate scenarios available; SSP119, SSP126, SSP245, SSP585. The Shared Socioeconomic Pathways (SSPs) are the standard for climate scenarios and portray different futures (Kriegler et al. 2014). These scenarios differ in the extent to which climate change is mitigated. To illustrate, SSP119 and SSP126 are high mitigation low greenhouse gas emission scenarios. SSP245 is a middle-of-the-road scenario with moderate mitigation and emissions. Lastly, SSP585 is a fossil-fueled future with high greenhouse gas emissions (Kriegler et al. 2014). By process of elimination the following ESMs were selected: CanESM5 (Swart et al. 2019), GFDL-ESM4 (John et al. 2018), MPI-ESM1-2-LR (Schupfner et al. 2021), KIOST-ESM (Kim et al. 2019). Of those four only KIOST-ESM did not have SSP119 and SSP126 available. For the validation against the actual observed reanalysis data, historical runs were used from 1998-2014. To complete the 25-year range, data from SSP245 was used for the years 2015-2022, as those were lacking in the historical runs. For all ESMs, the zonal (uas) and meridional (vas) surface wind components and the surface chlorophyll A concentration (chlos) were used for the standard model variant r1i1p1f1. All data was downloaded at the original model resolution before being regridded bilinearly to a 1° × 1° resolution in the same way as the ERA5 and ESACCI-OC data.

3.5. The Least Cost Path (LCP) Model

The LCP model used in this study is an adapted version of the one used in Skyllas et al. (in preparation). Even though the study by Skyllas et al. has not been published yet, the present study is based on the LCP model developed in Skyllas et al. (in preparation). The present study adapted the LCP model by moving from a seasonal to a daily resolution for wind data and a monthly resolution for chlorophyll A data. The least cost path model consists of a grid with a resolution of 1° × 1° and works as follows: the grid contains a starting location grid cell and a destination grid cell. To move from one grid cell to another has a certain cost. This cost depends on certain variables of the model, and in this model specifically on wind support, cross winds, distance, and food availability. There are many different paths to reach the destination from the starting grid. The least cost path model calculates the cost of each possible path and gives as output the path with the lowest total cost. Four separate cost grids are combined, to derive the total cost grid: one for the wind support, one for the

crosswinds, one for the chlorophyll, and one for the distance. In addition, a cost correction based on grid cell area is applied. Since the 1° × 1° grid cells distort zonally when moving to higher latitudes, geoCorrection from the gdistance package in R was applied to correct for this distortion (van Etten 2017).

The cost grid for wind consists of two parts: the tailwinds and the crosswinds. The first step is combining the zonal (u) and meridional (v) components of the wind into one wind vector ($\vec{c}$) field with both speed and direction. In order to calculate the wind support and cross wind the angle between the wind direction and the ground speed (θ) is taken resulting in Equation 1-6 and Figure 5:

(1) $wind\ speed = |\vec{c}|$

(2) $wind\ support = \vec{c}_{support} = |\vec{c}| \cdot \cos\theta$

Positive values for wind support indicate tailwinds, whereas negative values indicate headwinds. Since high wind support should have a low cost, the highest possible value of wind support, the 99th percentile, is subtracted from all wind support values and then the absolute value is taken (see Eq. 3). This way the highest wind support has a cost of 0, whereas low wind support has a high cost.

(3) $wind\ support\ cost = |wind\ support - 99th\ percentile\ of\ wind\ support|$

(4) $crosswind = \vec{c}_{cross} = |\vec{c}| \cdot \sin\theta$

For the crosswind the absolute value is taken, as it does not matter whether the cross wind is coming from left or right. On that account, crosswinds are always a hinderance for the tern and hence should have a positive cost.

(5) $ground\ speed = |\vec{a}|$

(6) $air\ speed = |\vec{b}| = \sqrt{(|\vec{a}| - \vec{c}_{support})^2 + \vec{c}_{cross}{}^2}$

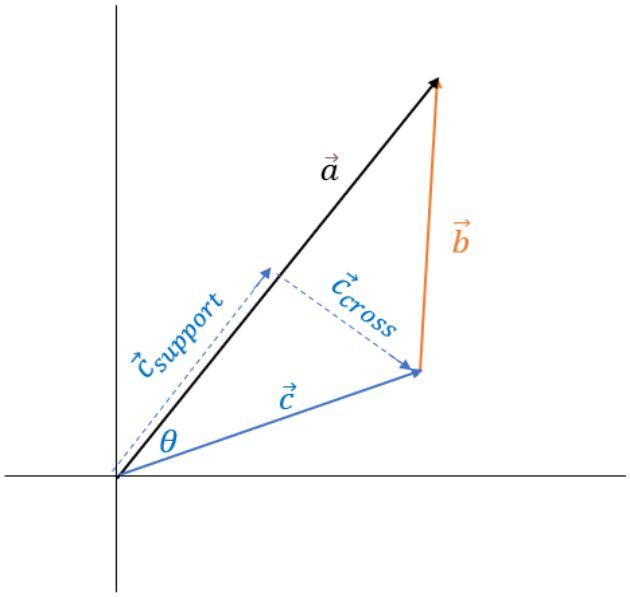

Figure 3. The groundspeed, windspeed, crosswind, and air speed vectors for a flying bird. Vector $\vec{a}$ is the groundspeed of the Arctic tern, the velocity compared to the surface (eq. 5). Vector $\vec{c}$ is the wind vector (eq. 1). The wind vector can be split into a support vector $\vec{c}_{support}$ (eq. 2) with the same direction as the ground speed vector, and a crosswind vector $\vec{c}_{cross}$ (eq. 4), perpendicular to the ground speed vector. The airspeed vector $\vec{b}$ (eq. 6), the displacement compared to the air due to work done by the bird, is calculated from the ground speed and wind support vectors.

Chlorophyll A data is heavily skewed, with a lot of grid cells with concentration values close to zero and only a few high values. The logarithmic is taken to account for this skewing and to increase the contrast between the relatively low chlorophyll concentrations. High chlorophyll concentrations still have a high logarithmic value but should have a low cost. Therefore, the cost is opposite to the logarithmic values, resulting in high chlorophyll concentrations having a low cost and low chlorophyll concentrations having a high cost. The last cost field comes from the distance and is the simplest of all cost fields. Since a correction for the spatial distortion of the grid cells is applied later, the initial distance cost field is completely uniform. Given that Arctic terns usually migrate over the ocean and not over land, grid cells with land masses were made inaccessible in the model preventing the Arctic terns from flying over land. Afterwards, all cost fields are normalized so that each cost field has the same mean cost per grid cell.

However, not all the factors of the cost fields are equally important. As explained in the section describing the migration strategies earlier, some terns put more weight on short migration distance, whereas others put more emphasis on high wind support. To put this difference in behavior of the terns into the model all the four cost fields were given a behavioral weight between 0 and 1, where the four weights combined should always add up to 1. The overall cost field is then a linear combination of these four factors with their respective behavioral weights. For the boreal spring migration of the Svalbard population, strong wind support is particularly important (Egevang et al. 2010, Hensz 2015, Hromádková et al. 2020, Skyllas et al. 2023). Therefore, the best 20 performing sets of weights for the boreal spring Svalbard population from Skyllas et al. (in preparation) were used in this study. Figure 6 lists the 20 sets of behavioral weights used in this study and illustrates that the Svalbard population has a high emphasis on tailwind support as supported by literature (Egevang et al. 2010, Hensz 2015, Hromádková et al. 2020, Skyllas et al. 2023). Per departure day 20 migration paths are simulated, each path corresponding with one set of the behavioral weights.

a) Wind support	b) distance	c) food availability	d) cross winds
0.9	0.0	0.0	0.1
0.9	0.0	0.1	0.0
0.9	0.1	0.0	0.0
0.8	0.0	0.0	0.2
0.8	0.2	0.0	0.0
0.8	0.1	0.1	0.0
0.8	0.1	0.0	0.1
0.8	0.0	0.1	0.1
0.7	0.3	0.0	0.0
0.7	0.1	0.2	0.0
0.7	0.0	0.1	0.2
0.6	0.0	0.0	0.4
0.6	0.4	0.0	0.0
0.6	0.0	0.2	0.2
0.6	0.0	0.1	0.3
0.5	0.4	0.1	0.0
0.5	0.0	0.3	0.2
0.5	0.3	0.1	0.1
0.5	0.0	0.2	0.3
0.5	0.1	0.2	0.2

Figure 6. All 20 sets of weights for the four behavioral factors used in this study. The total cost fields used in the LCP model are a linear combination of the four different behavioral factors (wind support, crosswind, food, distance) with their respective weight. These 20 sets were selected on performance in Skyllas et al. (in preparation). Varying all behavioral factors between 0 and 1 with steps of 0.1, gives a total of 195 unique combinations that have a sum of 1. In Skyllas et al. (in preparation) all 195 combinations were tested with seasonal mean data. The 20 sets with the lowest RMSE compared to the mean tracking data were selected.

3.6. Experiments

The LCP model was used for two sets of simulations. First, a sensitivity experiment exploring inter-individual variability, while randomizing various aspects of the migration was done. Model simulations were done with historical reanalysis data (ERA5 & ESACCI-OC), while randomizing certain aspects such as: starting location, departure day, and flight scheme. For the starting locations, locations were randomly drawn from a box in the Southern Atlantic Ocean with the coordinates between 60°W and 20°E, and 60°S and 80°S (see Figure 7). To illustrate the importance of the departure day, the departure day was uniformly randomized in the month of March of the respective year.

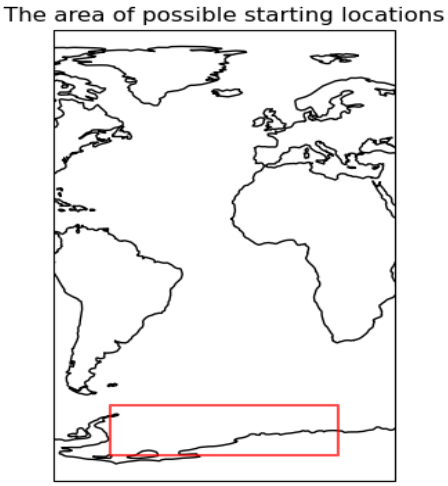

Figure 7. The red box (60°W - 20°E, 60°S - 80°S) highlights the area of possible starting locations during the starting location sensitivity experiment. The starting location was uniformly randomized: each point in the red box is equally likely to be the starting location.

The LCP model does not use the speed of the birds and therefore cannot exactly predict the birds' respective location on the migration path over time. To estimate the migration speed and hence the combination of location and time, the mean migration speed from tracking data (Fijn et al. 2013) was used in the main LCP model. However, this flight scheme of migrating about 400 kilometers per day is a very rough depiction of how the tern migrates. Some days the tern might fly 700 kilometers, whereas on other days the distance may be a mere 100 kilometers. To investigate the impact of a more realistic flight scheme, the migration speed per day was uniformly randomized per day between 100 and 700 kilometers until the destination was reached.

The second experiment explored how wind and chlorophyll patterns change in the future and the impact of this change on the migration route. In this experiment the LCP model was run with a fixed starting location based on the tracking data (23°W, 73°S) and a fixed flight scheme. Furthermore, the departure days were limited to five different departure days that were evenly spaced from the end of March until the end of April, which coincides with the departure date range in the tracking data. These aspects were fixed to limit the number of variables so that the influence of future changes could be explored more easily. However, as different periods in boreal spring have different wind and chlorophyll conditions, a limited selection of five starting days throughout spring was necessary to explore seasonal trends. The selected departure days were based on a previous study from Egevang et al. (2010), which found a departure window of April 12th – April 19th , and similar work from Hromádková et al. (2020), who found a departure window of March 31st – April 16th. The destination in this experiment was always the southern point of Svalbard: (15°E, 75°N).

The simulations were done for three time periods: historical from 1998 until 2022, a 30-year period ranging from 2036 until 2065, and a 30-year period at the end of the century from 2071 until 2100. For all periods the four selected ESMs were run with their available climate scenarios for the future: SSP119. SSP126, SSP245, SSP585. Each run had the aforementioned five starting days and 20 sets of behavioral weights, accounting for 100 migration paths per year per ESM (see Figure 8). In total there were 96500 migrations paths in this experiment.

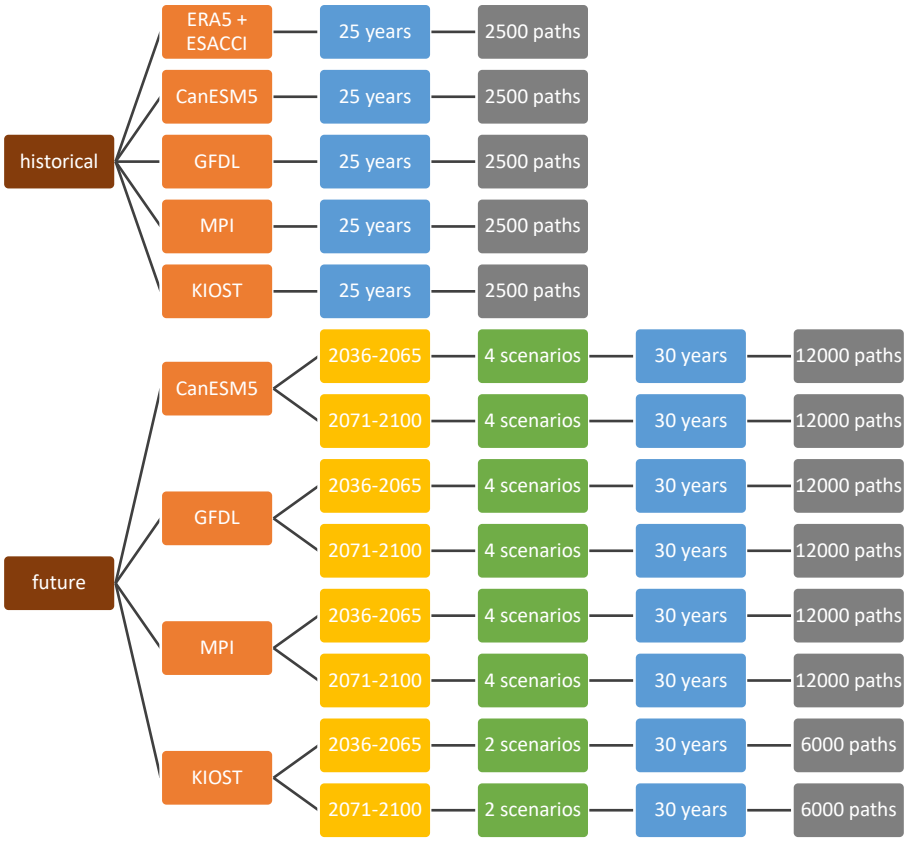

Figure 8. Overview of the model runs of the second set of simulations in this study. The second set of simulations consists of runs with historical data and runs with projected data in the future. In the historical part, top of the figure, the LCP model was run for reanalysis data and four ESMs. The runs were from 1998-2022. Every year had five different departure days evenly spaced between the end of March and the end of April. For every departure day the LCP model was run with the behavioral weights from Figure 6. The total amount of different migration routes per part of the simulations can be seen in the grey boxed on the right side. For the future simulations, the four ESMs were run for two time periods: 2036-2065 and 2071-2100. All available climate scenarios (SSP119, SSP126, SSP245, SSP585) available per ESM were used. For KIOST only SSP245 and SSP585 were available. Every year consisted of the same five departure days and the 20 behavioral weights, resulting in the total number of migration routes in the grey boxes.

Since wind pattern changes might be subtle, a good metric is needed to measure changes in future climate scenarios. The present study uses the northern bending point and the width of the S-shape (see Figure 4) as metrics. The northern bending point is defined as the latitude of the most westward point in the northern hemisphere. In cases where there is no singular point, but a most westward line of points, the most southerly latitude of the line was taken. The width of the S-shape is defined as the longitudinal difference between the most westward point in the northern hemisphere and the most eastward point in the southern hemisphere. These metrics were chosen because they can be linked to changes in strength of the wind pattern and the expansion of the Hadley cell. For example, if windspeeds of the southern westerlies and the trade winds decrease, the Arctic tern experiences less wind support. The longer path following these winds becomes less energy efficient and as a result

some terns will opt for a shorter (and straighter) path. This would decrease the width of the S-shape. In the same way, the northern bending point can be linked to the expansion of the Hadley cell. If the Hadley cell expands poleward, the Arctic terns will experience trade winds until higher latitudes. The point at which they change direction and make use of the tailwind from the westerlies, the northern bending point, will thus also shift poleward.

4. Results

4.1. Sensitivity

In order to explore the impact of the different components and future changes on the migration paths, the model and its sensitivity should first be examined. Compared to Skyllas et al. (in preparation) this study moved to a daily resolution for wind and monthly for chlorophyll. This allows for the present study to investigate the sensitivity and impact of multiple aspects of the migration that are not possible when seasonal means are used. Figure 9 shows the impact of different starting locations (upper left), different departure days (upper right), different flight schemes (lower left), and all of these combined (lower right). For the starting locations, locations were randomly drawn from a box in the Southern Atlantic Ocean with the coordinates between 60°W and 20°E, and 60°S and 80°S (see Figure 7). Randomizing the starting location gave three possible paths:

A) a relatively straight line along the coast of Africa and Europe
B) following a path along the coast of South America before crossing the Atlantic Ocean towards Svalbard
C) the “normal” S-shape following the wind pattern.

The results of this first experiment demonstrate that the first option mainly occurred with starting locations on the eastside of the defined box. The second option was mainly observed for starting locations on the far westside of the box. Finally, the majority of terns starting in the middle of the box followed the S-shape.

To illustrate the importance of the departure day, the departure day was uniformly randomized in the month of March of the respective year, with each day in March equally likely to be the starting day. The departure day gives a broad band of S-shapes, indicating that the departure day is a key factor in the migration path and determining the shape of the path (see Figure 9b).

To investigate the impact of a more realistic flight scheme, the migration speed per day was uniformly randomized per day between 100 and 700 kilometers (see Figure 9c). The different flight schemes do not seem to be very important in the model, as they give the same S-shape flight paths as with randomizing the departure day, but with less variance.

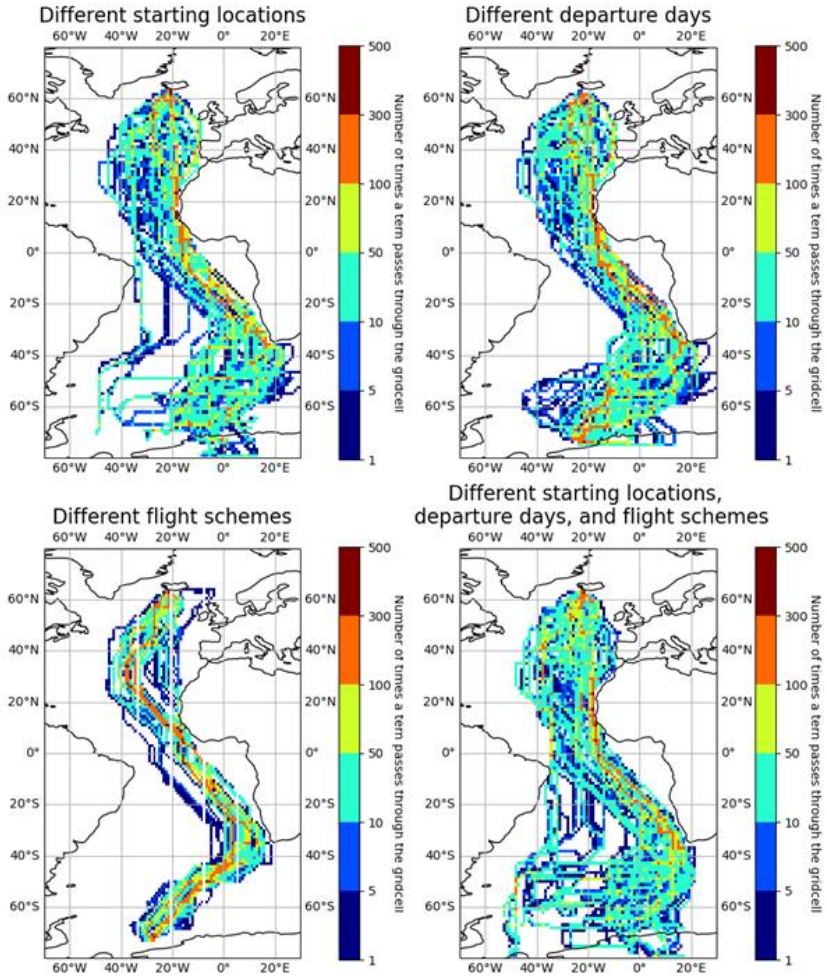

Figure 9. Migration paths for the year 2022. Per panel different sources for variability in the migration route were randomized. 9a: Randomized starting locations: starting locations were randomized according to figure 7. 9b: randomized departure days: starting days were uniformly randomized between March 1st and March 30th . 9c: randomized flight schemes: per simulation, the migration speed was randomized per day between 100km and 700km until the destination was reached. 9d: randomized starting locations, departure days, and flight schemes.

Combining the starting location, departure day, and flight schemes gives rise to a lot of variability between the three types of paths and also per type of path. Together these types can accommodate for differences in behavior between individual birds and populations. The standard deviation per sensitivity experiment gives a good indication which of the three aforementioned aspects of the migration is the most important for the Arctic tern. The higher the standard deviation, the more the migration routes differ when altering the respective aspect (e.g. starting location). The departure day had a mean standard deviation of 7.19° of longitude, whereas the different flight schemes had a mean standard deviation of 3.83° of longitude. The resulting paths are more sensitive to the starting date than to the flight scheme. The starting location had a mean standard deviation of 9.57° of longitude. This high standard deviation is partly imposed by the high variability in starting locations. Nevertheless, this indicates that starting location is a major factor for the Arctic tern, which is not surprising given that the total migration distance can change significantly with the starting location. Finally, the starting location, departure day, and flight scheme together had a mean standard deviation of 11.47° of longitude. This is comparable to the mean standard deviation of the tracking data (see Figure 4), which has a mean standard deviation of 10.58°, indicating that the starting location, departure day, and flight scheme together have a variability similar to that of individual Arctic tern behavior.

4.2. The present

The starting location, departure day, and flight scheme together cause a huge amount of variability in the tracks. In order to keep the number of changing variables to a minimum, this variability was limited to better explore present day trends and the impact of future changes. Therefore, the starting location and flight scheme were fixed, and the departure day was limited to five different days. Nevertheless, the daily, interannual, and decadal variability, and the behavior of the Arctic terns together, still allow paths across the entire Atlantic Ocean to occur (see Figure 10a).

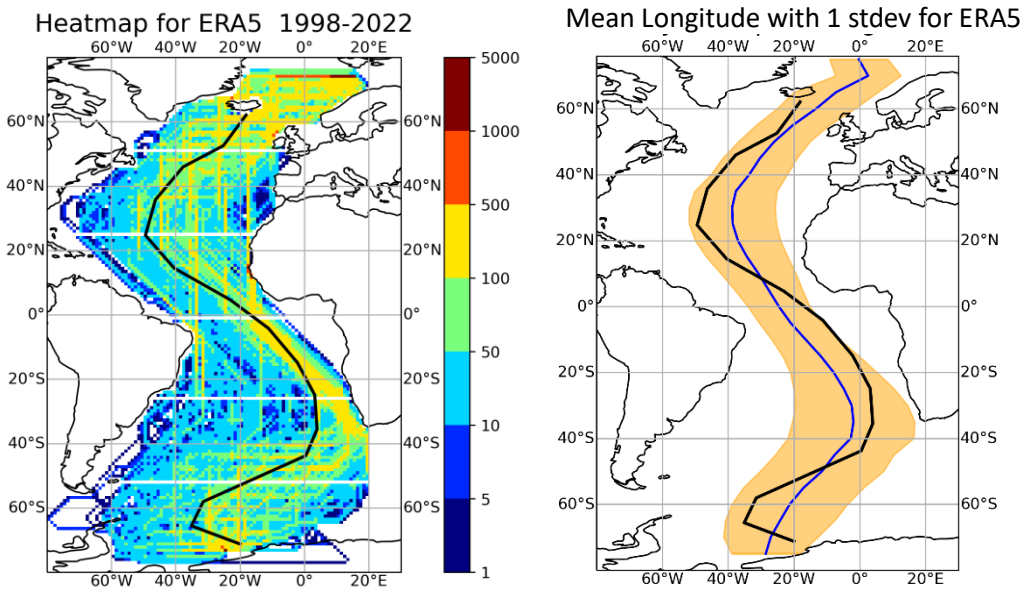

Figure 10. The left panel shows a heatmap of the modeled Arctic terns for the years 1998-2022 with ERA5 wind data. In total there were 2500 tern migration paths modeled. The black line shows the mean position of the Arctic tern tracking data. The variability here is higher than in figure 9 due to interannual and interdecadal variability. In the right panel the blue line shows the mean longitude per latitude band of 5° of those 2500 migrations. The orange band is a 1 standard deviation band from the mean. The black line is again the mean of the Arctic tern tracking data.

The number of simulations makes plotting all the migration paths and, albeit to a lesser extent, heatmaps rather ineffective to analyze the data. The mean migration path and its RMSE compared to the tracking data or the migration path from reanalysis data (ERA5 & ESACCI-OC) provides a good indication of the performance of the model per ESM. The ERA5 reanalysis data with ESACCI gives the lowest RMSE of 8.56° of longitude compared to the tracking data (see Figure 11b). CanESM5 and GFDL perform the best of the ESMs with a respective RMSE of 9.56° and 9.79° of longitude compared to the tracking data. MPI differs the most from the tracking data with a RMSE of 11.72° of longitude. It is important to note that the ESMs are far closer to ERA5 than to the tracking data, with a RMSE of only a few degrees of latitude for CanESM5 and GFDL. It is also worth noting that KIOST and MPI differ more from ERA5 and the tracking data. This difference can be attributed to their straighter path, mainly in the Southern Atlantic Ocean (see Figure 9a). On the other hand, CanESM5 and GFDL have an S-shape that is more comparable to that of ERA5. However, all ESMs and ERA5 have a significantly straighter path than the tracking data, resulting in a high RMSE.

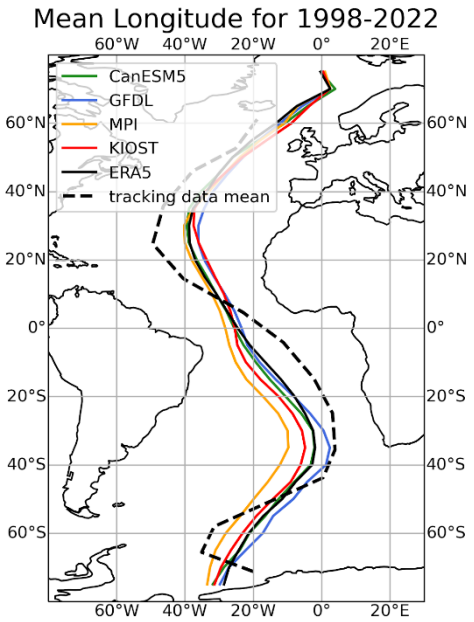

	RMSE compared to ERA5 (°longitude)	RMSE compared to The tracking data (° longitude)
CanESM5	1.54	9.56
GFDL	2.44	9.79
MPI	5.51	11.72
KIOST	3.02	10.64
ERA5	0.00	8.56

Figure 11. 11a: The mean migration path for four different ESMs in color, with the tracking data as black line, and ERA5 as black dashed line. 11b: The RMSE of the mean migration path for the four different ESMs and ERA5 compared to ERA5, and the tracking data mean migration path. The RMSE is calculated per 5° of latitude, and only up until the northern most point of the tracking data (Iceland).

The difference in shape between ESMs on the one hand, and the tracking data and, to a lesser extent, ERA5 on the other hand, could have multiple reasons. The differences between ERA5 and the ESMs is rooted in the difference between the wind and chlorophyll fields (see Figure 11&12). The zonal component of the wind in the North Atlantic next to the coast of Canada is stronger in the ESMs than in ERA5. However, for the majority of the rest of the North Atlantic Ocean the ERA5 zonal component is significantly stronger than the ESMs. This is especially prevalent in CanESM5, MPI and KIOST. This trend might play a role in the straighter path that MPI and KIOST have compared to ERA5.

For the meridional component, the ESMs are weaker northward along the coast of Patagonia, whereas in the middle of the Southern Atlantic Ocean between Patagonia and South-Africa the ESMs are stronger northward. This aligns with the straighter paths of MPI and KIOST, but not with the similar paths that CanESM5 and GFDL have. MPI has the strongest meridional component in the central northern part of the Atlantic Ocean, which aligns with having the straightest migration path. The other ESMs predominantly have a stronger northern component of the meridional wind vector along the coast of Canada. The difference maps of chlorophyll A concentration demonstrate that most ESMs have a higher mean concentration in the polar region of the Northern Atlantic (see Figure 12c). The difference maps also demonstrate that GFDL and CanESM5 in general have slightly higher concentrations than ESACCI-OC, whereas MPI has significantly enhanced chlorophyll concentration levels. Furthermore, MPI has a relatively high productive region next to the west coast of Africa. This could lead certain terns to adjust their path to cross this productive region and benefit from the abundance of food in this area. This leads to lower grid cell costs in the LCP model, which makes it more likely for the modeled Arctic terns to take a straight path along the coast of Africa. Consequently, the mean migration path for MPI would shift eastward and become straighter. The former eastward trend is not observed, while the latter is observed with MPI having the straightest, defined as the longitudinal difference between the eastern most point in the southern hemisphere and the western most point in the northern hemisphere, migration path.

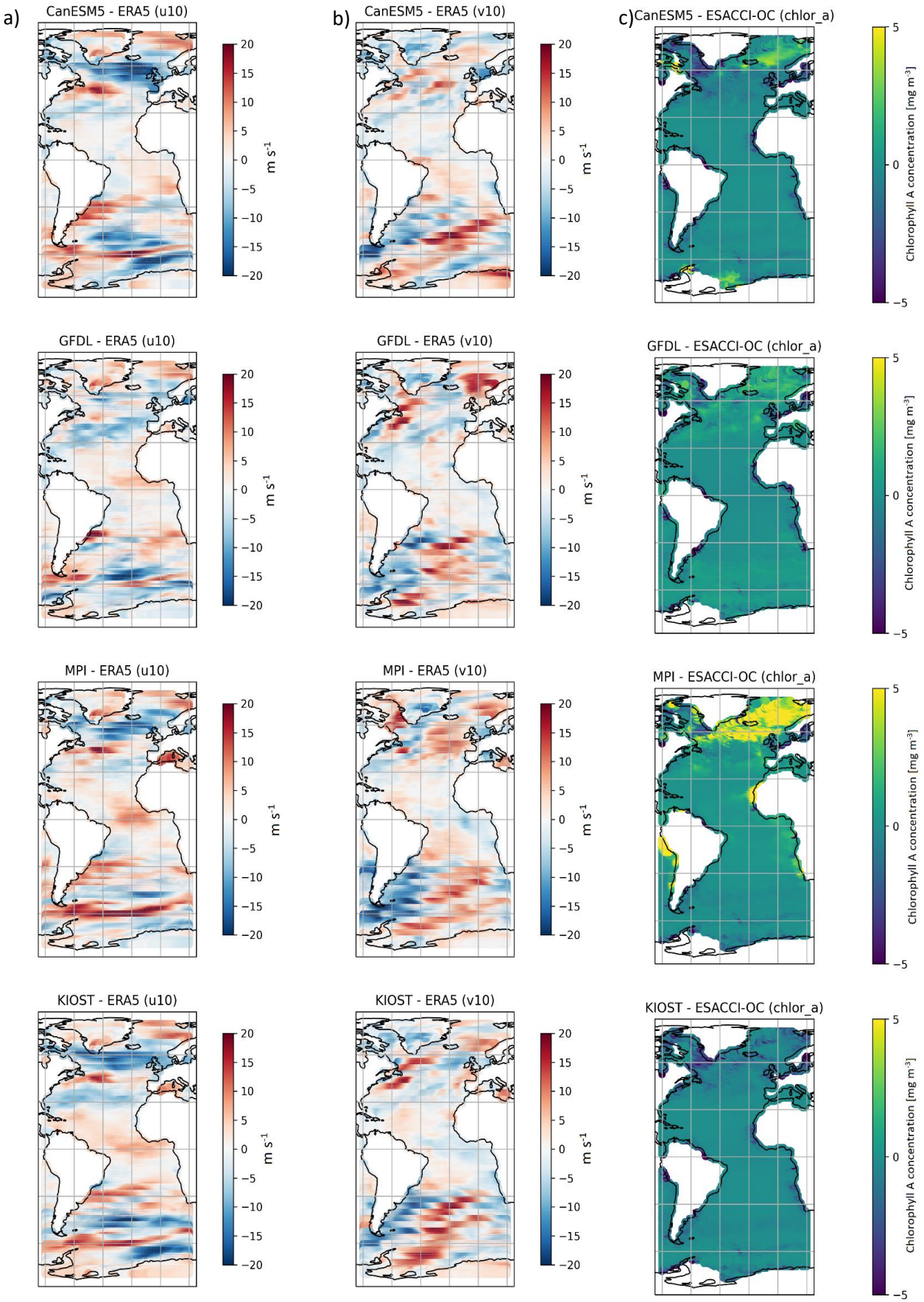

Figure 12. Difference maps between the ESMs and ERA5 for the zonal (u10) and meridional (v10) component of the wind in 12a and 12b. The difference maps between the ESMs and ESACCI-OC for the chlorophyll concentration in 12c. All difference maps are for the historical period 1998-2022.

The differences between the wind and chlorophyll fields of the ESMs and the reanalysis data shed some light on the discrepancy between the migration paths of two. Most differences in migration path can be explained by the difference in the zonal wind field. For example, MPI and KIOST have a straighter and more direct migration path compared to ERA5. The zonal wind difference maps highlight that MPI and KIOST have weaker trade winds in the southern hemisphere and weaker westerlies in the northern hemisphere compared to ERA5. Therefore, due to lower wind support while making an S-shape, the migration path with the least cost for MPI and KIOST is more reliant on a shorter migration distance, resulting in a straighter path.

However, the wind and chlorophyll fields cannot motivate the difference between ESMs and the Arctic tern tracking data. Even though the wind conditions that the tracked Arctic terns experienced during their migration were most likely different from the wind fields from the ESMs or ERA5, there is no way to quantify this since the tracking data only consists of observations of the position of the Arctic terns. Furthermore, the difference in migration path between the tracked terns and the ESMs is significantly bigger than the difference between the modeled paths from ERA5 and the ESMs. Therefore, it is likely that the different atmospheric conditions, which we cannot quantify, are not the only cause for the different migration paths between the tracked terns and the modeled ESM paths. A possible explanation for this could be that the 20 behavioral weight sets used in the simulations do not accurately cover the behavior of the tracked terns. When comparing the selectivity of tailwinds, there was a clear difference between very high emphasis on tailwind support and moderate emphasis on tailwind support (see Figures 13 & 14). It is noteworthy to recall that behavioral weights with low emphasis on tailwind support, tailwind factors < 0.5, were already left out. A very high emphasis on tailwind support with tailwind factor ≥ 0.8 gives a more pronounced and more frequent S-shape. In contrast, a moderate emphasis on tailwind with tailwind factor ≤ 0.7 has a lower frequency of S-shaped paths and a higher frequency of straight paths along the coast of Africa or South America. The turning point at which the Arctic terns started to take a straight path more frequently is approximately at a tailwind factor of 0.7. Only considering paths with high tailwind selectivity leads to a smaller RMSE compared to the tracking data in all ESMs. This is especially prevalent in the northern hemisphere, where the terns take more advantage of the trade winds and westerlies, resulting in a more pronounced curve (see Figure 14). A precise tailwind factor for the tracked Arctic terns cannot be estimated since this differs per individual tern. However, based on the findings with high emphasis on tailwind support, the tailwind factor for the Svalbard population of Arctic terns can be estimated to be between 0.7 and 1.

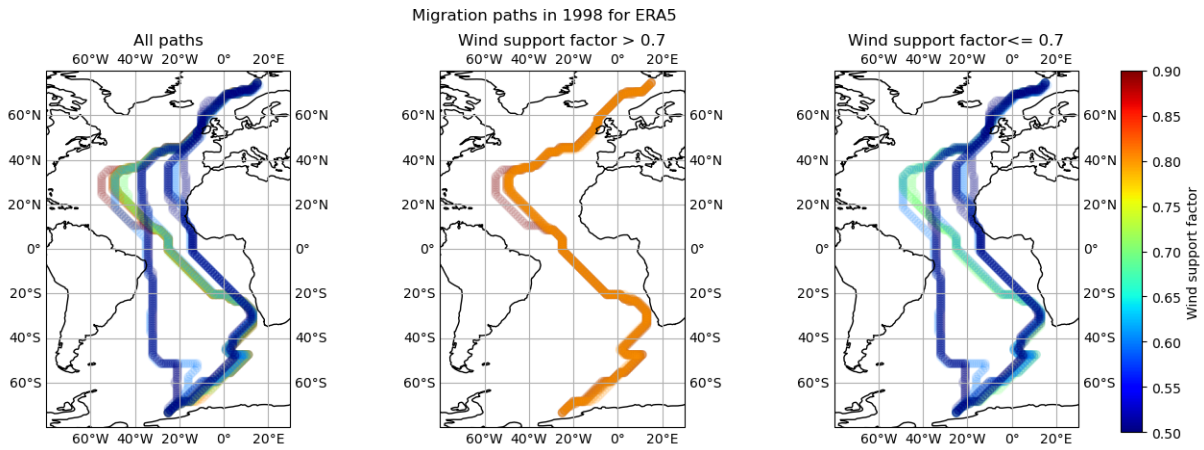

Figure 13. The migration paths for ERA5 data for the year 1998. The left panel, 13a has all 100 migration paths color-coded for the value of the tailwind factor. The middle panel, 13b only has the migration paths with very high wind support factors of 0.8 or 0.9. The right panel, 13c only has the migration paths with wind support factors between 0.5 and 0.7. 11b,c show that high wind support factors result in S-shaped migration routes.

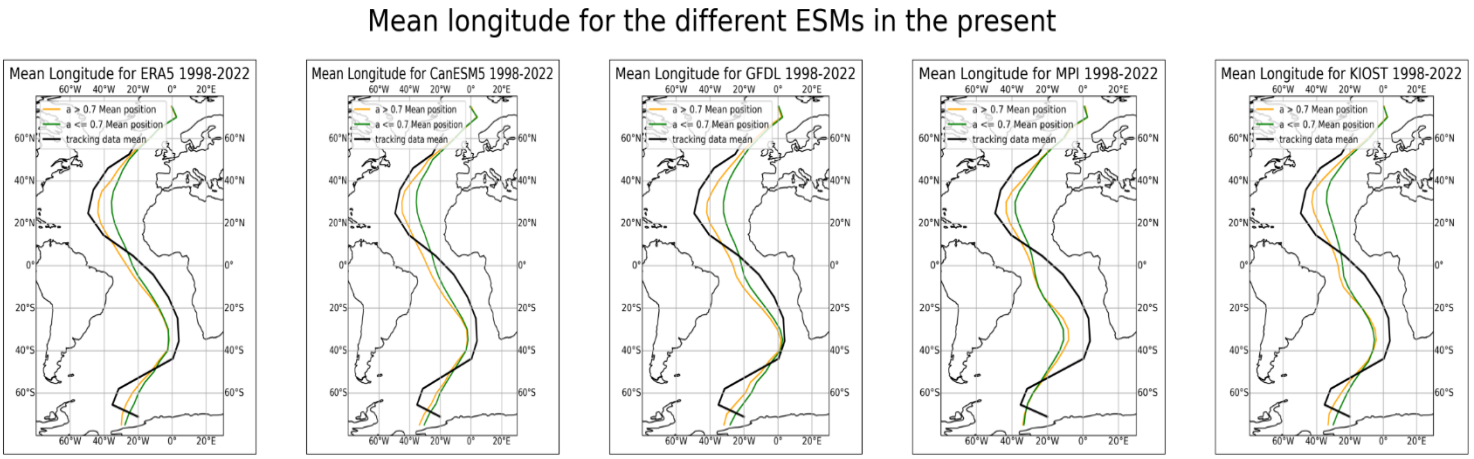

Figure 14. The green line is the mean migration path for only moderate wind support factors (0.5, 0.6, 0.7). The orange line is the mean migration path for only very high wind support factors (0.8, 0.9). The black line is the mean migration path from the tracking data. From left to right you have ERA5, CanESM5, GFDL, MPI, and KIOST. High wind support factors result in a mean migration route closer to the tracking data compared to moderate wind support factors.

In addition to the tailwind selectivity, the departure day could also be an explanation for the discrepancy between tracking data and model output based on ESM input. The departure window for optimal wind conditions during the migration could be small. The migration paths of five different starting days (March 27th/week 1, April 3rd/week 2, April 10th/week 3, April 17th/week 4, April 24th/ week 5) were analyzed. No clear optimal departure week was found (see Figure 15). Where week 4 was often closest to the tracking data in the northern hemisphere, it was often furthest away from the tracking data in the southern hemisphere. Week 3 had a similar pattern but vice versa. The departure day appears to be relatively important for the migration path, but it is mainly seen in an east-west shift of the migration path. It is noteworthy to recall that the used departure days fall within the departure window from Egevang et al. (2010) and Hromádková et al. (2020).

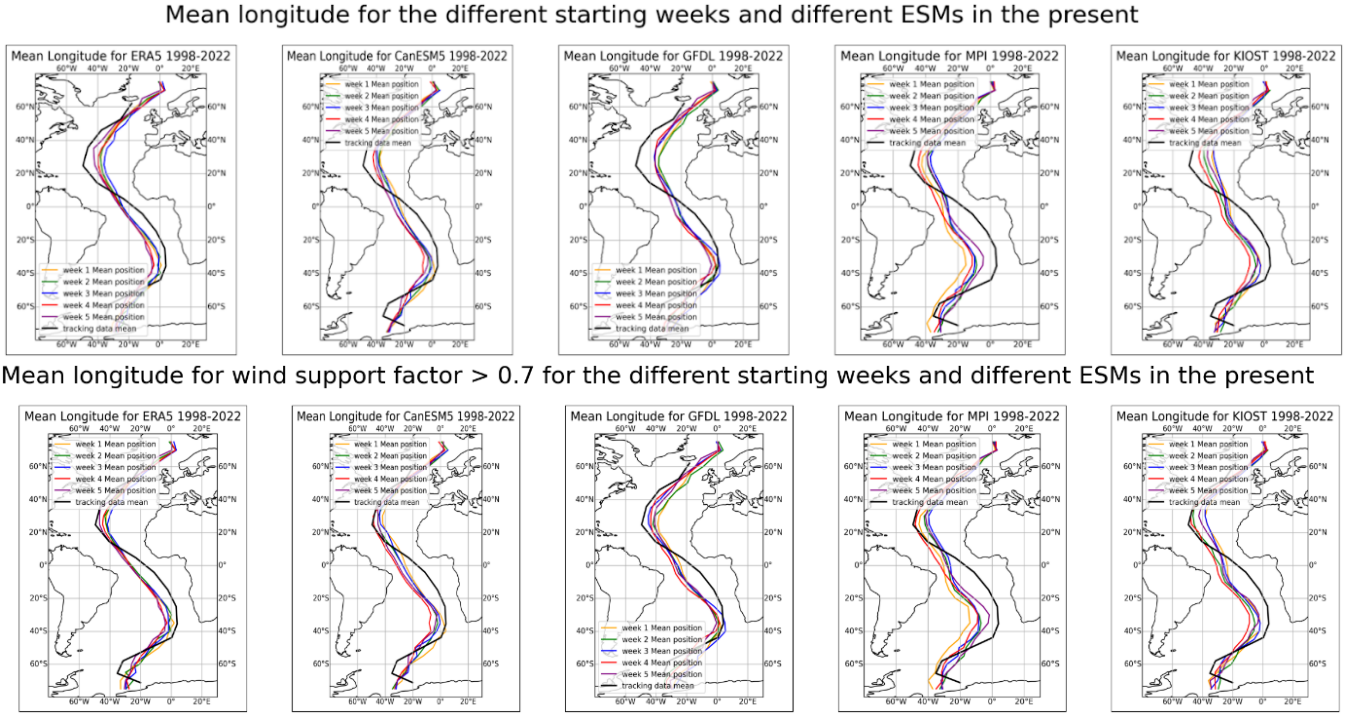

Figure 15. Top: the mean migration paths per departure day. The departure days are evenly spaced from the end of March until the end of April. The first departure day, March 27th, is referred to as week 1, the second departure day, April 3rd as week 2 etc. Bottom: the mean migration paths per departure day, but only paths with high wind selectivity are considered. From left to right: ERA5, CanESM5, GFDL, MPI, KIOST.

4.3. Future Changes

4.3.1. Global Pattern Shifts

The four different SSPs have very different projections of GHG concentrations during the 21st century. This difference cannot be recognized in the migration paths, however. In fact, compared to the start of the century, there was very little visual change in the migration paths at the end of century in the model ensemble (see Figure 16). A trend in the migration paths ranging from relatively low to high emission scenarios is not clearly present. The only minimal change occurs in the southern hemisphere. Due to increased zonal wind components of the westerlies, the migration path shifts a few degrees eastward until the first change of direction at approximately 30-40°S. In the northern hemisphere no significant differences were found between mean migration paths at the start and end of the century.

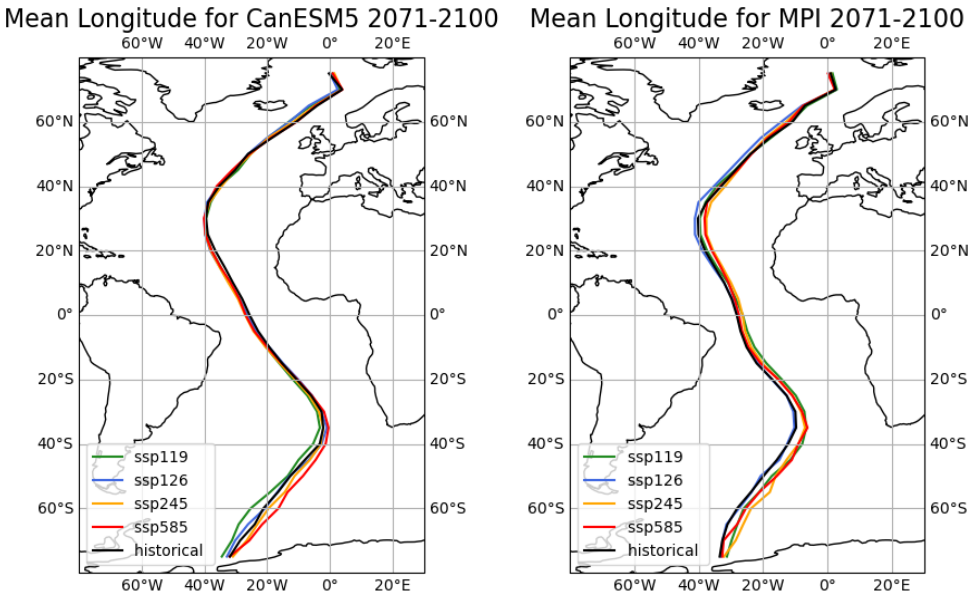

Figure 16. The mean migration paths at the end of the century for four different SSPs in CanESM5 (left) and MPI (right). Only minimal changes between SSP scenarios are observed.

4.3.2. Northern Bending Point

The Arctic terns benefit from a strong tailwind provided by the dominant trade winds that carry them from the west coast of the lower part of Africa towards the coast of North America. How long they can benefit from these strong tailwinds depends on the extend of the Hadley cell. If the Hadley cell expands poleward, the Arctic terns could benefit longer from the trade winds before changing direction. Accordingly, the northern bending point in the migration path would shift poleward. This trend of the northern bending point shifting poleward was not observed (see Figure 17). The change in northern bending point differs per ESM and per scenario, and no clear trend between ESMs or scenarios was found. Furthermore, these results are insignificant since the minimal changes in northern bending point are well within the standard deviations. Therefore, the results show no poleward shift of the northern bending point and consequently do not give an indication for expansion of the Hadley cell.

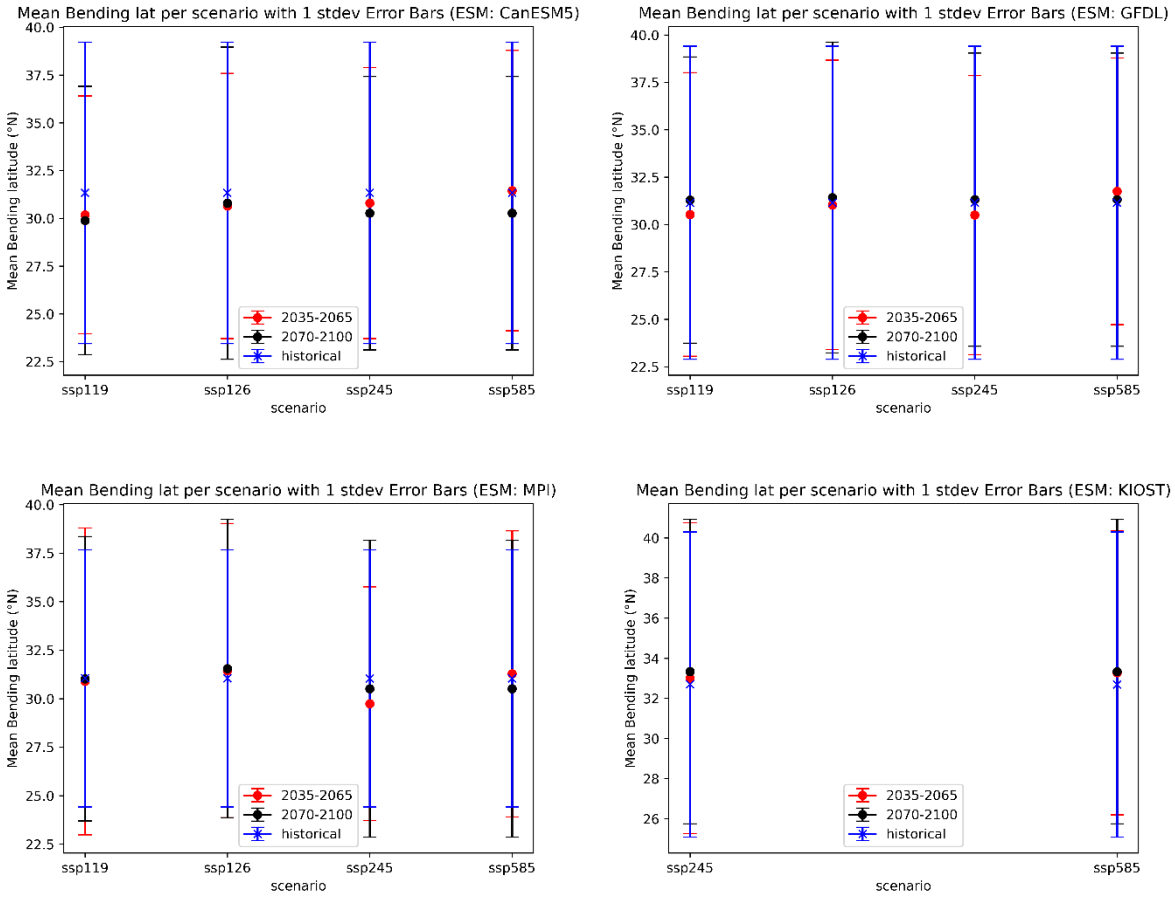

Figure 17. The northern bending point, the latitude of the most westward longitude in the northern hemisphere, for 1998-2022 (blue), 2036-2065 (red), and 2071-2100 (black). The four different SSPs are in different panels: top left: CanESM5, top right: GFDL, bottom left: MPI, bottom right: KIOST.

4.3.3. S-Shape

The width of the S-shape of the migration path differs significantly in the model ensemble (see Figure 18). In GFDL and CanESM5 the terns make use of the relatively strong westerlies in the southern part of the Atlantic Ocean, before benefiting from the trade winds in the middle part of the S-shaped migration path. Even though the path is longer, the presence of tailwind support leads to a lower cumulative migration cost. This results in a “wide” S-shape where the difference between the eastern most point and the western most point of the migration is relatively large. In MPI on the other hand, the trade winds are significantly less strong. The Arctic tern can benefit less from the winds by following a wide S-shape. The lack of tailwind support means that the cumulative migration cost is often higher than taking a straight path. Accordingly, the longer S-shaped path is not beneficial in this case and the terns are more likely to opt for a straighter path. This process causes a relatively narrow S-shape.

No future change in the width of the S-shaped migration path was found (see Figure 18). The change of the width of the S-shape differs per ESM and per scenario, and no clear trend between ESMs or scenarios was identified. Furthermore, these results are insignificant since the minimal changes in the width of the S-shape are well within the standard deviations. Therefore, the results show no change in the width of the S-shaped migration path and consequently do not give an indication for a change in strength of the wind pattern.

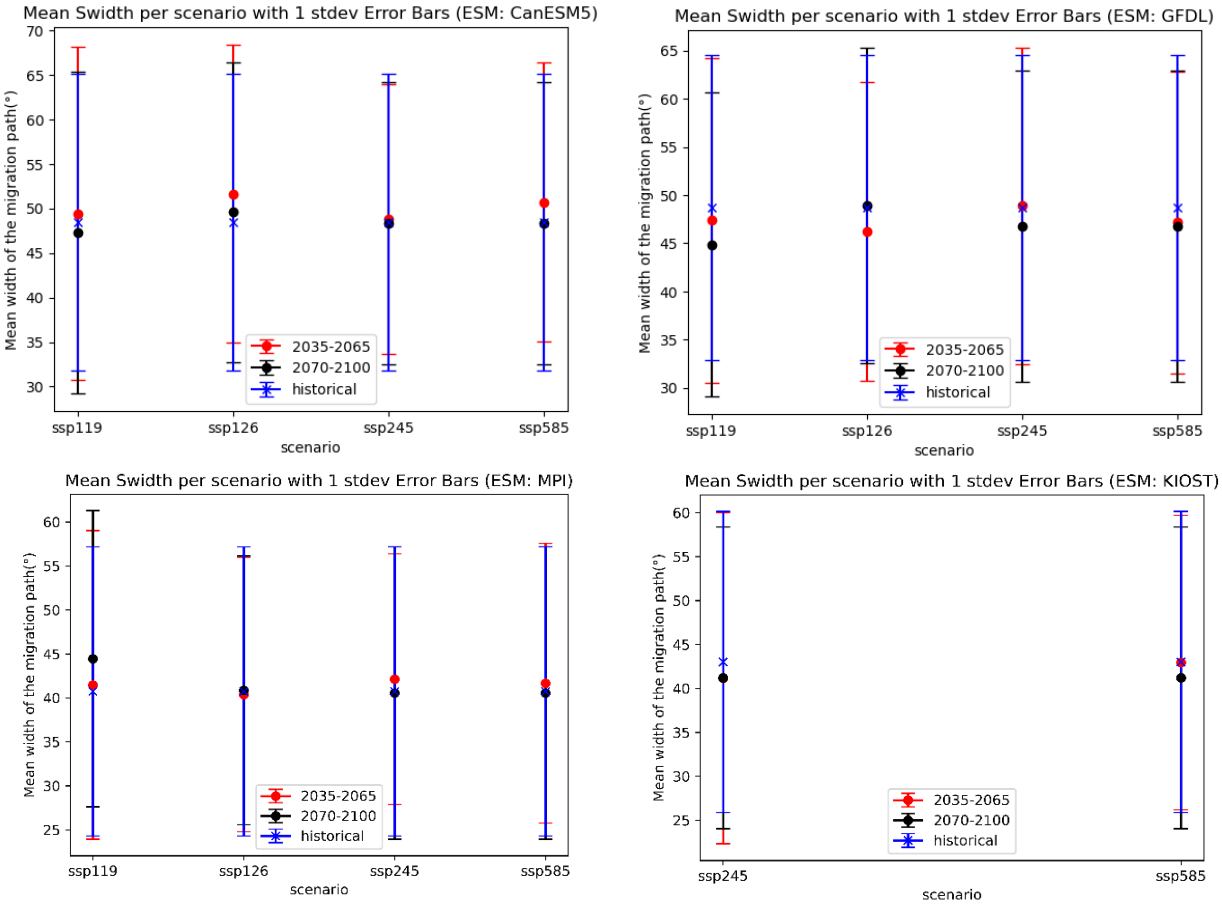

Figure 18. The width of the S-shape, the longitudinal difference between most eastern point in the southern hemisphere and the most western point in the northern hemisphere, for 1998-2022 (blue), 2036-2065 (red), and 2071-2100 (black). The four different SSPs are in different panels: top left: CanESM5, top right: GFDL, bottom left: MPI, bottom right: KIOST.

However, the wind fields of the ESM ensemble do project changes in windspeeds at the end of the century. Figure 19 shows the zonal mean of projected changes in windspeed at the end of the century compared to the start of the century for the ESM ensemble. What stands out in figure 19 is the increase in strength of the zonal component of westerly winds between 50°S-80°S. At the same time, the meridional component decreases in strength. Furthermore, in the northern hemisphere the zonal component in both the trade winds, between 0°N-20°N, and the westerlies, between 30°N-50°N, decrease in strength. This illustrates that, even though only minimal and insignificant changes were found in the migration path, the wind patterns are projected to change.

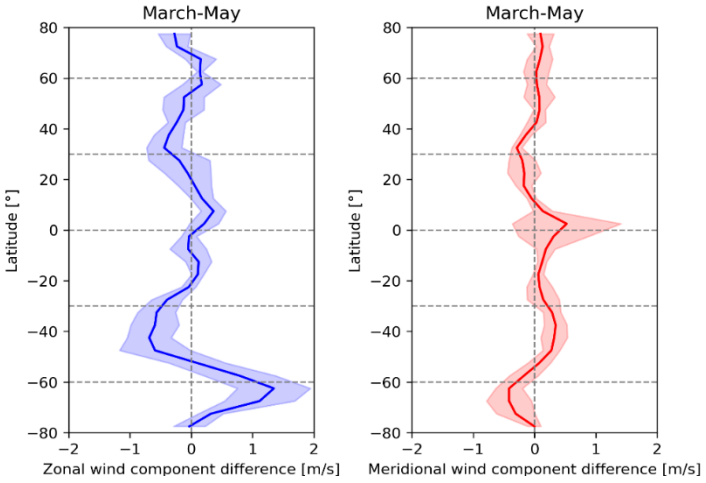

Figure 19. The zonal mean of projected changes in windspeed per 5° latitude bins in the period March to May. The colored lines are the mean projected change of the ESM ensemble. The shaded area is the standard deviation of the ESM ensemble. On the left in blue is the projected change of the zonal wind component. Positive values indicate a more eastward zonal component. On the right in red is the projected change of the meridional wind component. Positive values indicate a more northward meridional component.

5. Discussion

Based on a large number of location data and LCP model simulations, the present study has attempted to investigate the influence of wind patterns on the boreal spring migration route of Arctic terns to Svalbard. As mentioned in the introduction, there are a number of factors that influence the migration route of Arctic terns. Tailwinds are key in the migration of Arctic terns, but when and where the terns can benefit from tailwind depends on starting location, departure day, flight scheme, and behavior. When all these factors are accounted for, three main migration routes were found for the modeled Arctic terns (Hensz 2015, Hromádková et al. 2020). The first route is straight alongside the east coast of South America before crossing the Atlantic Ocean, minimizing the distance in the southern hemisphere and using the tail- and crosswinds to drift to the other side of the Atlantic in the northern hemisphere. The second route goes straight alongside the west coast of Africa and Europe, minimizing the migration distance while also benefitting from upwelling areas along the coast of Africa. This route is similar to the Arctic tern population that nests in the North Sea area. The final and dominant S-shaped route follows the wind pattern entirely. The latter route is characterized by first relying on the westerlies to drift to the west coast of Africa, then changing direction on the flow of the trade winds while drifting towards North America, and finally changing direction again and making use of the westerlies in the northern hemisphere. The Arctic terns experience tailwinds throughout the entirety of this route.

While validating the LCP model with a daily wind resolution against the tracking data, it became apparent that not all of the 20 sets of behavioral factors could produce migration routes similar to the tracking data. This finding is in contrast with previous studies that modelled the migration route using a seasonal resolution, such as in Skyllas et al. (in preparation). When going from a seasonal mean wind field to daily wind fields, Arctic terns need to adapt more due to more variable and unpredictable conditions. In the seasonal mean the westerlies and trade winds are very clear and pronounced, as the used wind field is the average over the season. In reality however, mainly the westerlies are not present every day. To compensate for this, the modelled Arctic terns from the present study have demonstrated that a behavioral change with a higher emphasis on tailwind selectivity is necessary to produce the observed tracking paths. In conclusion, the intrinsic value of the tailwind selectivity factor is higher when shifting from a seasonal to daily resolution.

The importance of the departure window has been emphasized in numerous studies (Chapman et al. 2011, Hensz 2015, Hedenström and Akesson 2016, Hromádková et al. 2020, Skyllas et al. 2023). Though the departure day was relevant for the migration path in the LCP model of the present study, a clear optimal departure window was not observed. This could potentially be attributed to ESMs not having an accurate representation of seasonal changes in wind patterns in their models. Another explanation could be the way in which the daily resolution was incorporated in the LCP model. The migration speed of the terns was fixed in the model, thus not giving the modelled terns the chance to adapt to major changes in atmospheric conditions (Hedenström and Akesson 2016). In the case of extremely favorable atmospheric conditions the terns could not speed up and fly a longer distance per day. Reversely, the terns could not rest or refuel during poor atmospheric conditions waiting for better conditions before resuming their migration. A final explanation for the lack of a clear departure window could be that the total cost of the migration was not analyzed. A clear departure window could potentially arise when comparing the total energetic cost of the migration per departure day.

While looking at the performance of individual ESMs from the ensemble, CanESM5 and GFDL were best suited to simulate the Arctic tern migration path for historical data. MPI and KIOST were less suited for this purpose as they had difficulty simulating a wide enough S-shape frequently, resulting in

a migration path significantly straighter than the tracking data. This can mainly be attributed to weaker trade winds in the tropical regions compared to other models.

After validating and fine-tuning the model for ESM data, the future scenarios were analyzed. This proved to be a challenging task as changes were small between scenarios and time periods. This was especially prevalent for the difference between scenarios, which turned out to be unexpectedly small. The uncertainty in the migration path can mainly be attributed to differences in ESMs, departure days and Arctic tern behavior. This illustrates that the representation of the climate system still varies a lot between ESMs and that the changes in wind pattern and the uncertainty of the future climate are less important than the differences between ESMs. This is in line with previous findings from Bichet et al. (2012), who argue that future wind pattern changes are small, and Smith et al. (2020), who argue that ESMs do not properly represent the predictability of the North Atlantic climate.

No clear poleward shift of the northern bending point and, consequently, no indication for expansion of the Hadley cell was found. Furthermore, no future change in the width of the S-shaped migration path was observed. The present study has identified that the future trends in the migration path changes are not significant due to a high standard deviation. Accordingly, the results of this study fall outside of the confidence interval. These results are in line with previous findings from Bichet et al. (2012), who demonstrated that the simulated impact on global wind patterns over oceans are small and not always significant.

Finally, the LCP model of the present study has indicated that the changes in the wind patterns have no straightforward impact on the migration route of Arctic terns. The LCP model has demonstrated that the wind pattern changes were small, and the predominant migration path is close to the same. This finding is consistent with that of Skyllas et al. (in preparation) and Morten et al. (2023). However, the total cost of the migration was not addressed, as it is not (yet) incorporated in the LCP model. The LCP model only simulates the path with the lowest cost for the given circumstances. Over time the path with the lowest cost might not change, but the circumstances and therefore the total cost for migration could. Keeping the same migration path might cost more (or less) energy in the future, as more compensation or drifting is needed for the optimal path. Another possible scenario could be a change of destination. Not only the conditions for migration are changing, but also nesting conditions, such as snow cover, precipitation, and abundance of food at the destination are changing. The changing conditions at the destination together with a higher or lower cost for migration could lead to a change of destination, departure time and migration route. Finally, the Arctic terns might evolve and adapt to changing conditions, which also could influence their migration route.

In conclusion, if assumed that the destination and behavior of the Arctic terns do not change, the migration route of Arctic terns will stay the same, outside of minimal changes.

5.1. Limitations

This study used an ensemble of only four ESMs due to limited data availability. If more ESMs would have both daily wind data and monthly chlorophyll data available for SSP scenarios, a more diverse ESM ensemble could have been used. Moreover, this would allow for ESM selection based on performance in accordance with Skyllas et al. (2023). The ESM models are an immensely complex representation of our climate system, and therefore come with a variety of uncertainties. Together with the limited understanding of certain processes, most notably the future development of wind patterns and chlorophyll A as a proxy for food availability, this can lead to significant differences and uncertainties between models, as highlighted by Smith et al. (2020). Furthermore, the geolocators

come with an uncertainty of ~185 km. Therefore, the model could not perform on a higher resolution and had to be run on the coarse resolution of 1°x 1°, needing the wind and chlorophyll data to be scaled to a coarser grid.

The resolution of ESMs can significantly impact their performance. To resolve mesoscale eddies and Rossby waves, ESMs require a high resolution. Due to the coarse resolution of the Arctic tern tracking data, the ESMs could not be validated at high resolution. The ESMs used in this study therefore had a low resolution and were limited in resolving eddies and Rossby waves accurately and instead had to use parametrizations that do not represent all the dynamics of eddies. As eddies are projected to shift poleward with climate change, this could lead to major changes in wind patterns. Especially in the mid-latitudes, the representation of eddies in ESMs could have a strong impact on the resulting wind patterns.

Another limitation of the longitude latitude grid with resolution 1°x 1°, is the zonal distortion that occurs when moving poleward. The present study tried to limit the impact of this spatial grid cell distortion on the simulations by applying a correction factor from the gdistance package in R (van Etten 2017). However, this correction is not perfect and could lead to erroneous results at high latitudes. Moving from a rectangular latitude longitude grid to a hexagonal grid would solve this issue and is therefore a recommended improvement of the LCP model.

The incorporation of food availability could also be a limitation to the LCP model. Firstly, a monthly resolution of chlorophyll A was used due to lack of satellite coverage for shorter time periods. However, coarse temporal resolution of chlorophyll A compared to wind could influence the results. Secondly, chlorophyll A is a proxy for phytoplankton concentration and mainly acts as an indication of productive marine areas. Using other, more direct, indicators of food availability for Arctic terns, such as Net Primary Production or nekton data, could improve accuracy of food availability for Arctic terns. In this study chlorophyll A was used, as it was readily available for current and future projections over the entire Atlantic area.

Ringing Arctic terns with geolocators is a difficult and time-consuming task. Accordingly, there is only a small number of ringed Arctic terns that provide data about their migration tracks. The model was validated against this Arctic tern tracking data, but the low sample size of the tracking data could lead to biases. The geolocators could only log the location until Iceland due to the nature of the geolocators with the diurnal cycle. The validation of the migration routes to Svalbard of the model could thus only be validated until Iceland, potentially paving the way for further biases.

Lastly, the LCP model itself combines multiple factors of variability: interannual variability, decadal variability, different departure days, and behavioral weights. Each have their own uncertainty and combining them in the LCP model leads to a cascade of uncertainty. This resulted in high variability demonstrated by the standard deviations.

5.2. Outlook

This study has focused mainly on the near surface level wind patterns with a 2D-model. However, migrating birds fly in a three-dimensional space. Upgrading the model to 3D could give more insight into migration altitudes and would allow for more complex wind patterns to influence the migration. Different wind speed and direction at different altitude levels might significantly change how accurate models can simulate their migration route. For Arctic terns, geolocators are used because they are small and light. Existing trackers with altimeters are often too big or heavy for an Arctic tern to carry. Tracking studies with other birds already exist and demonstrate different migration altitudes per species (Lindström et al. 2021, Sjöberg et al. 2021). If GPS trackers become available for Arctic terns,

this could give a compelling insight into their migration altitudes as observations indicate that they can migrate at altitudes between tens of meters above the surface until 5 kilometers above the surface (Alerstam et al. 2007). For the LCP model in the current form, adding the vertical dimension and improving the resolution of the tracking data would not be computationally efficient. The search of appropriate values for the behavioral parameters is now done with brute force. The increase in amount of grid cells would make this process time consuming and computationally inefficient. Instead, future studies could use a machine learning approach to train the model with existing data to find the optimal (range for) behavioral parameter values.

Acknowledgements

I am very grateful to Nomikos Skyllas and Richard Bintanja for their guidance, help, feedback, suggestions, comments on my draft, and weekly meetings at KNMI throughout the project. Nomikos in particular, for his incredible dedication and patience, always being ready to help and making the LCP model and data from his research available. Furthermore, I would like to thank Mo Verhoeven for his feedback on research directions. I am thankful to Erik van Sebille and Michiel Baatsen for supervising my project from inside the UU, their feedback throughout the project, and the comments on the original draft. Finally, I would like to thank my family, in particular Romy Coers, for their emotional support, suggestions and feedback throughout the year.

References

Abell, J., Winckler, G., Anderson, R., Herbert, T. (2021). Poleward and weakened westerlies during Pliocene warmth. Nature 589, 70–75. https://doi.org/10.1038/s41586-020-03062-1

Alerstam, T., & Gudmundsson, G. (1999). Migration Patterns of Tundra Birds: Tracking Radar Observations along the Northeast Passage. Arctic, 52, 346-371. https://doi.org/10.14430/ARCTIC941

Alerstam, T., Bäckman, J., Gudmundsson, G., Hedenström, A., Henningsson, S., Karlsson, H., Rosén, M., Strandberg, R. (2007). A polar system of intercontinental bird migration. Proceedings of the Royal Society B: Biological Sciences, 274, 2523 - 2530. https://doi.org/10.1098/rspb.2007.0633

Alerstam, T. (2011). Optimal bird migration revisited. *J Ornithol* 152 (Suppl 1), 5–23. https://doi.org/10.1007/s10336-011-0694-1

Archer, C., & Caldeira, K. (2008). Historical trends in the jet streams. Geophysical Research Letters, 35(8).

Ashmole, N. (1968). BODY SIZE, PREY SIZE, AND ECOLOGICAL SEGREGATION IN FIVE SYMPATRIC TROPICAL TERNS (AVES: LARIDAE). Systematic Biology, 17, 292-304. https://doi.org/10.1093/SYSBIO/17.3.292

Bellido, J., Brown, A., Valavanis, V., Giráldez, A., Pierce, G., Iglesias, M., Palialexis, A. (2008). Identifying essential fish habitat for small pelagic species in Spanish Mediterranean waters. Hydrobiologia, 612, 171-184. https://doi.org/10.1007/s10750-008-9481-2

Bichet, A., Wild, M., Folini, D., Schär, C. (2012). Causes for decadal variations of wind speed over land: Sensitivity studies with a global climate model. Geophysical Research Letters, 39. https://doi.org/10.1029/2012GL051685

Canion, A., MacIntyre, H., Phipps, S. (2013). Short-term to seasonal variability in factors driving primary productivity in a shallow estuary: Implications for modeling production. Estuarine Coastal and Shelf Science, 131, 224-234. https://doi.org/10.1016/J.ECSS.2013.07.009

Chakraborty, D., Saha, S., Singh, R. (2015). Change in Near-Surface Wind Velocity: What Implications will it have on Ecosystem and Agriculture?. Current Science, 108, 761-761. https://doi.org/10.18520/CS/V108/I5/761-761

Chapman, J., Klaassen, R., Drake, V.A., Fossette, S., Hays, G., Metcalfe, J., Reynolds, A., Reynolds, D., Alerstam, T. (2011). Animal orientation strategies for movement in flows. Curr. Biol. 21, R861–R870

Chapman, J., Nilsson, C., Lim, K., Bäckman, J., Reynolds, D., Alerstam, T. (2016). Adaptive strategies in nocturnally migrating insects and songbirds: contrasting responses to wind. The Journal of animal ecology, 85(1), 115–124. https://doi.org/10.1111/1365-2656.12420

D'Agostino, R., Lionello, P. (2017). Evidence of global warming impact on the evolution of the Hadley Circulation in ECMWF centennial reanalyses. Clim Dyn 48, 3047–3060. https://doi.org/10.1007/s00382-016-3250-0

Deng, K., Azorin-Molina, C., Yang, S., Hu, C., Zhang, G., Minola, L., Chen, D. (2022). Changes of Southern Hemisphere westerlies in the future warming climate,Atmospheric Research,Volume 270, 106040, ISSN 0169-8095, https://doi.org/10.1016/j.atmosres.2022.106040

Druon, J., Hélaouët, P., Beaugrand, G., Fromentin, J., Palialexis, A., Hoepffner, N. (2019). Satellite-based indicator of zooplankton distribution for global monitoring. Scientific Reports, 9. https://doi.org/10.1038/s41598-019-41212-2

Egevang, C., Stenhouse, I., Phillips, R., Petersen, A., Fox, J., Silk, J. (2010). Tracking of Arctic terns Sterna paradisaea reveals longest animal migration. Proceedings of the National Academy of Sciences of the United States of America, 107(5), 2078–2081. https://doi.org/10.1073/pnas.0909493107

Encounter Edu. Global Atmospheric Circulation. Retrieved from: https://encounteredu.com/cpd/subject-updates/learn-about-global-atmospheric-circulation [retrieved on: 02-12-2023]

van Etten J. (2017). "R Package gdistance: Distances and Routes on Geographical Grids." Journal of Statistical Software, 76(13), 1-21. doi:10.18637/jss.v076.i13

Ferrari, R., & Ferreira, D. (2011). What processes drive the ocean heat transport. Ocean Modelling, 38, 171-186. https://doi.org/10.1016/J.OCEMOD.2011.02.013

Fijn, R., Hiemstra, D., Phillips, R., Winden, J. (2013). Arctic Terns Sterna paradisaea from the Netherlands Migrate Record Distances Across Three Oceans to Wilkes Land, East Antarctica., 101, 12-3. https://doi.org/10.5253/078.101.0102

Gray, W., Lavergne, C., Wills, R., Menviel, L., Spence, P., Holzer, M., Kageyama, M., Michel, E. (2021). Poleward shift in the Southern Hemisphere westerly winds synchronous with the deglacial rise in CO2. Goldschmidt2021 abstracts. https://doi.org/10.21203/RS.3.RS-404786/V1

Grise, K., Davis, S., Staten, P., Adam, O. (2018). Regional and Seasonal Characteristics of the Recent Expansion of the Tropics. Journal of Climate, 31(17), 6839-6856. https://doi.org/10.1175/JCLI-D-18-0060.1

Grise, K., Davis, S., Simpson, I., Waugh, D., Fu, Q., Allen, R., Rosenlof, K., Ummenhofer, C., Karnauskas, K., Maycock, A., Quan, X., Birner, T., Staten, P. (2019). Recent Tropical Expansion: Natural Variability or Forced Response?. Journal of Climate, 32(5), 1551-1571. https://doi.org/10.1175/JCLI-D-18-0444.1

Grise, K., & Davis, S. (2020). Hadley cell expansion in CMIP6 models, Atmos. Chem. Phys., 20, 5249–5268, https://doi.org/10.5194/acp-20-5249-2020

Grotjahn, R. (2002). "BAROCLINIC INSTABILITY | University of California, Davis, CA, USA Copyright Elsevier Science Ltd. doi:10.1006/rwas.2002.0076

Hedenström, A. & Akesson, S. (2016). Ecology of tern flight in relation to wind, topography and aerodynamic theory. Philosophical Transactions of The Royal Society B Biological Sciences. 371. 10.1098/rstb.2015.0396

Hensz, C. (2015). Environmental factors in migratory route decisions: a case study on Greenlandic Arctic Terns (Sterna paradisaea). Animal Migration, 2(1), 76-85. https://doi.org/10.1515/ami-2015-0004

Herrera, E., & Morett, S. (2016). On the direction of Coriolis force and the angular momentum conservation. Revista Brasileira de Ensino de Física, 38.

Hersbach, H., Bell, B., Berrisford, P., Biavati, G., Horányi, A., Muñoz Sabater, J., Nicolas, J., Peubuy, P., Radu, R., Rozum, I., Schepers, D., Simmons, A., Soci, C., Dee, D., Thépaut, J. N. (2018). ERA5 hourly data on single levels from 1979 to present. *Copernicus climate change service (c3s) climate data store (cds)*, *10*(10.24381)

Hoskins, B., Yang, G., Fonseca, R. (2020). The detailed dynamics of the June–August Hadley Cell. Quarterly Journal of the Royal Meteorological Society, 146, 557 - 575. https://doi.org/10.1002/qj.3702

Hoskins, B., & Yang, G. (2021). The Detailed Dynamics of the Hadley Cell. Part II: December–February. Journal of Climate, 34(2), 805-823. https://doi.org/10.1175/JCLI-D-20-0504.1

Hromádková, T., Pavel, V., Flousek, J., Briedis, M. (2020). Seasonally specific responses to wind patterns and ocean productivity facilitate the longest animal migration on Earth. Marine Ecology Progress Series. 638. 10.3354/meps13274

Hsu, C., Liu, W., Wurtele, M. (1997). Impact of Scatterometer Winds on Hydrologic Forcing and Convective Heating through Surface Divergence. Monthly Weather Review, 125, 1556-1576. https://doi.org/10.1175/1520-0493(1997)125<1556:IOSWOH>2.0.CO;2

Hu, Y., & Zhou, C. (2010). Decadal changes in the Hadley circulation. In Advances in Geosciences: Volume 16: Atmospheric Science (AS) (pp. 61-74).

Hu, Y., Huang, H., Zhou C. (2018). Widening and weakening of the Hadley circulation under global warming. Science Bulletin, Volume 63, Issue 10,Pages 640-644,ISSN 2095-9273, https://doi.org/10.1016/j.scib.2018.04.020

Huang, R., Chen, S., Chen, W., Hu, P., Yu, B. (2019). Recent Strengthening of the Regional Hadley Circulation over the Western Pacific during Boreal Spring. Adv. Atmos. Sci. 36, 1251–1264. https://doi.org/10.1007/s00376-019-9004-2

Intergovernmental Panel on Climate Change (IPCC). (2014). Climate Change 2014: Synthesis Report. Contribution of Working Group I to the Fifth Assessment Report of the Intergovernmental Panel on Climate Change: The Physical Science Basis. Geneva, Switzerland.

Intergovernmental Panel on Climate Change (IPCC). (2021). Climate Change 2021: The Physical Science Basis. Contribution of Working Group I to the Sixth Assessment Report of the Intergovernmental Panel on Climate Change. Geneva, Switzerland.

Intergovernmental Panel on Climate Change (IPCC). (2022): Annex II: Glossary [Möller, V., van Diemen R., Matthews J., Méndez C., Semenov S., Fuglestvedt J., Reisinger A.]. In: Climate Change 2022: Impacts, Adaptation and Vulnerability. Contribution of Working Group II to the Sixth Assessment Report of the Intergovernmental Panel on Climate Change [Pörtner H., Roberts D., Tignor M., Poloczanska E., Mintenbeck K., Alegría A., Craig M., Langsdorf S., Löschke S., Möller V., Okem A., Rama B.]. Cambridge University Press, Cambridge, UK and New York, NY, USA, pp. 2897–2930, doi:10.1017/9781009325844.029

John, J., Blanton, C., McHugh, C., Radhakrishnan, A., Rand, K., Vahlenkamp, H., Wilson, C., Zadeh, N., Dunne, J., Dussin, R., Horowitz, L., Krasting, J., Lin, P., Malyshev, S., Naik, V., Ploshay, J., Shevliakova, E., Silvers, L., Stock, C., Winton, M., Zeng, Y. (2018). NOAA-GFDL GFDL-ESM4 model output prepared for CMIP6. Earth System Grid Federation. https://doi.org/10.22033/ESGF/CMIP6.8706

Kemp, M., Shamoun-Baranes, J., van Loon, E., McLaren, J., Dokter, A., Bouten, W. (2012). Quantifying flow-assistance and implications for movement research. Journal of theoretical biology, 308, 56–67. https://doi.org/10.1016/j.jtbi.2012.05.026

Kim, Y., Noh, Y., Kim, D., Lee, M., Lee, H., Kim, S., Kim, D. (2019). KIOST KIOST-ESM model output prepared for CMIP6.Earth System Grid Federation. https://doi.org/10.22033/ESGF/CMIP6.11249

Kriegler, E., O'Neill, B., Riahi, K., Ebi, K., Hallegatte, S., Carter, T., Mathur, R., van Vuuren, D. (2014). A New Scenario Framework for Climate Change Research: The Concept of Shared Socioeconomic Pathways. Climatic Change. 122. 10.1007/s10584-013-0905-2

Laliberté, F., Zika, J., Mudryk, L., Kushner, P., Kjellsson, J., Döös, K. (2015). Constrained work output of the moist atmospheric heat engine in a warming climate. Science, 347, 540 - 543. https://doi.org/10.1126/science.1257103

Lavigne, H., D'Ortenzio, F., d'Alcalà, M., Claustre, H., Sauzède, R., Gačić, M. (2015). On the vertical distribution of the chlorophyll a concentration in the Mediterranean Sea: a basin scale and seasonal approach. Biogeosciences, 12, 5021-5039. https://doi.org/10.5194/BG-12-5021-2015

Liechti, Felix. (2006). Birds: Blowin' by the wind?. Journal of Ornithology. 147. 202-211. 10.1007/s10336-006-0061-9

Lindström, A., Alerstam, T., Andersson, A., Bäckman, J., Bahlenberg, P., Bom, R., Ekblom, R., Klaassen, R., Korniluk, M., Sjöberg, S., Weber, J. (2021). Extreme altitude changes between night and day during marathon flights of great snipes, Current Biology, Volume 31, Issue 15, Pages 3433-3439.e3, ISSN 0960-9822, https://doi.org/10.1016/j.cub.2021.05.047

Lu, J., Vecchi, G., Reichler, T. (2007). Expansion of the Hadley cell under global warming. Geophysical Research Letters, 34. https://doi.org/10.1029/2006GL028443

Mcknight, A., Allyn, A., Duffy, D., Irons, D. (2013). 'Stepping stone' pattern in Pacific Arctic tern migration reveals the importance of upwelling areas. Marine Ecology Progress Series. 491. 253-264. 10.3354/meps10469

McLaren, J., Shamoun-Baranes, J., Bouten, W. (2012). Wind selectivity and partial compensation for wind drift among nocturnally migrating passerines. Behavioral ecology: official journal of the

International Society for Behavioral Ecology, 23(5), 1089–1101. https://doi.org/10.1093/beheco/ars078

Morten, J., Buchanan, P., Egevang, C., Glissenaar, I., Maxwell, S., Parr, N., Screen, J., Vigfúsdóttir, F., Vogt-Vincent, N., Williams, D., Williams, N., Witt, M., Hawkes, L., Thurston, W. (2023). Global warming and arctic terns: Estimating climate change impacts on the world's longest migration. Global change biology, 29(19), 5596–5614. https://doi.org/10.1111/gcb.16891

O'Brien, E. (2019). Balancing the Potential Vorticity Seesaw: The Bare Essentials of Baroclinic Instability. Earth Syst Environ 3, 341–351. https://doi.org/10.1007/s41748-019-00128-7

Phillips, R., Silk, J., Croxall, J., Afanasyev, V., Briggs, D. (2004). Accuracy of geolocation estimates for flying seabirds. Marine Ecology Progress Series, 266, 265-272

Randall, D. (2015). An introduction to the global circulation of the atmosphere. Princeton University Press.

Sathyendranath, S., Jackson, T., Brockmann, C., Brotas, V., Calton, B., Chuprin, A., Clements, O., Cipollini, P., Danne, O., Dingle, J., Donlon, C., Grant, M., Groom, S., Krasemann, H., Lavender, S., Mazeran, C., Mélin, F., Müller, D., Steinmetz, F., Valente, A., Zühlke, M., Feldman, G., Franz, B., Frouin, R., Werdell, J., Platt, T. (2023): ESA Ocean Colour Climate Change Initiative: Global chlorophyll-a data products gridded on a geographic projection at 4km resolution, Version 6.0. NERC EDS Centre for Environmental Data Analysis, 28-11-2023. https://doi.org/10.5285/5011d22aae5a4671b0cbc7d05c56c4f0

Schupfner, M., Wieners, K., Wachsmann, F., Milinski, S., Steger, C., Bittner, M., Jungclaus, J., Früh, B., Pankatz, K., Giorgetta, M., Reick, C., Legutke, S., Esch, M., Gayler, V., Haak, H.,de Vrese, P., Raddatz, T., Mauritsen, T., von Storch, J., Behrens, J., Brovkin, V., Claussen, M., Crueger, T., Fast, I., Fiedler, S., Hagemann, S., Hohenegger, C., Jahns, T., Kloster, S., Kinne, S., Lasslop, G., Kornblueh, L., Marotzke, J., Matei, D., Meraner, K., Mikolajewicz, U., Modali, K., Müller, W., Nabel, J., Notz, D., Peters-von Gehlen, K., Pincus, R., Pohlmann, H., Pongratz, J., Rast, S., Schmidt, H., Schnur, R., Schulzweida, U., Six, K., Stevens, B., Voigt, A., Roeckner, E. (2021). DKRZ MPI-ESM1.2-LR model output prepared for CMIP6. Earth System Grid Federation. https://doi.org/10.22033/ESGF/CMIP6.15575

Shamoun-Baranes, J., van Loon, E., Liechti, F., Bouten, W. (2007). Analyzing the effect of wind on flight: pitfalls and solutions. The Journal of experimental biology, 210(Pt 1), 82–90. https://doi.org/10.1242/jeb.02612

Shamoun-Baranes, J., Liechti, F., Vansteelant, W. (2017). Atmospheric conditions create freeways, detours and tailbacks for migrating birds. Journal of comparative physiology. A, Neuroethology, sensory, neural, and behavioral physiology, 203(6-7), 509–529. https://doi.org/10.1007/s00359-017-1181-9

Schulzweida, U. (2021) Climate Data Operator User Guide (Version 2.0.0) DOI:10.5281/zenodo.1435454

Sjöberg, S., Malmiga, G., Nord, A., Andersson, A., Bäckman, J., Tarka, M., Willemoes, M., Thorup, K., Hansson, B., Alerstam, T., Hasselquist, D. (2021). Extreme altitudes during diurnal flights in a nocturnal songbird migrant. Science372,646-648. DOI:10.1126/science.abe7291

Skyllas, N., Loonen, M., Bintanja, R. (2023). Arctic tern flyways and the changing Atlantic Ocean wind patterns, Climate Change Ecology, Volume 6, 2023, 100076, ISSN 2666-9005, https://doi.org/10.1016/j.ecochg.2023.100076

Smith, D., Scaife, A., Eade, R., Athanasiadis, P., Bellucci, A., Bethke, I., Bilbao, R., Borchert, L., Caron, L., Counillon, F., Danabasoglu, G., Delworth, T., Doblas-Reyes, F., Dunstone, N., Estella-Perez, V., Flavoni, S., Hermanson, L., Keenlyside, N., Kharin, V., Kimoto, M., Merryfield, W., Mignot, J., Mochizuki, T., Modali, K., Monerie, P., Müller, W., Nicolì, D., Ortega, P., Pankatz, K., Pohlmann, H., Robson, J., Ruggieri, P., Sospedra-Alfonso, R., Swingedouw, D., Wang, Y., Wild, S., Yeager, S., Yang, X., Zhang, L. (2020). North Atlantic climate far more predictable than models imply. Nature, 583, 796 - 800. https://doi.org/10.1038/s41586-020-2525-0

Staten, P., Lu, J., Grise, K., Davis, S., Birner, T. (2018). Re-examining tropical expansion. Nature Clim Change 8, 768–775. https://doi.org/10.1038/s41558-018-0246-2

Staten, P., Grise, K., Davis, S., Karnauskas, K., Waugh, D., Maycock, A., Fu, Q., Cook, K., Adam, O., Simpson, I., Allen, R., Rosenlof, K., Chen, G., Ummenhofer, C., Quan, X., Kossin, J., Davis, N., Son, S. (2020). Tropical Widening: From Global Variations to Regional Impacts. Bulletin of the American Meteorological Society, 101(6), E897-E904. https://doi.org/10.1175/BAMS-D-19-0047.1

Studholme, J., & Gulev, S. (2018). Concurrent Changes to Hadley Circulation and the Meridional Distribution of Tropical Cyclones. Journal of Climate, 31(11), 4367-4389. https://doi.org/10.1175/JCLI-D-17-0852.1

Swart, N., Cole, J., Kharin, K., Lazare, M., Scinocca, J., Gillett, N., Anstey, J., Arora, V., Christian, J., Jiao, Y., Lee, W., Majaess, F., Saenko, O., Seiler, C., Seinen, C., Shao, A., Solheim, L., von Salzen, K., Yang, D., Winter, B., Sigmond, M. (2019). CCCma CanESM5 model output prepared for CMIP6. Earth System Grid Federation. https://doi.org/10.22033/ESGF/CMIP6.3682

Waugh, D., Sobel, A., Polvani, L. (2017). What Is the Polar Vortex and How Does It Influence Weather?. Bulletin of the American Meteorological Society, 98(1), 37-44. https://doi.org/10.1175/BAMS-D-15-00212.1

Wills, R., White, R., Levine, J. (2019). Northern Hemisphere Stationary Waves in a Changing Climate. Curr Clim Change Rep 5, 372–389. https://doi.org/10.1007/s40641-019-00147-6

Winn, C., Campbell, L., Christian, J., Letelier, R., Hebel, D., Dore, J., Fujieki, L., Karl, D. (1995). Seasonal variability in the phytoplankton community of the North Pacific Subtropical Gyre. Global Biogeochemical Cycles, 9, 605-620. https://doi.org/10.1029/95GB02149

Witman, J., Cusson, M., Archambault, P., Pershing, A., Mieszkowska, N. (2008). The relation between productivity and species diversity in temperate-Arctic marine ecosystems.. Ecology, 89 11 Suppl, S66-80 . https://doi.org/10.1890/07-1201.1

Zeng, Z., Ziegler, A., Searchinger, T., Yang, L., Chen, A., Ju, K., Piao, S., Li, L., Ciais, P., Chen, D., Liu, J., Azorín-Molina, C., Chappell, A., Medvigy, D., Wood, E. (2019). A reversal in global terrestrial stilling and its implications for wind energy production. Nature Climate Change, 9, 979-985. https://doi.org/10.1038/s41558-019-0622-6

Zhang, Z., Wang, K., Chen, D., Li, J., Dickinson, R. (2019). Increase in Surface Friction Dominates the Observed Surface Wind Speed Decline during 1973–2014 in the Northern Hemisphere Lands. Journal of Climate. https://doi.org/10.1175/JCLI-D-18-0691.1